Molecular tuning of sea anemone stinging

Lily S He[1], Yujia Qi[2], Corey AH Allard[1], Wendy A Valencia-Montoya[1,3], Stephanie P Krueger[1], Keiko Weir[1], Agnese Seminara[2#], Nicholas W Bellono[1#]

[1]Department of Molecular and Cellular Biology, Harvard University, Cambridge MA 02138 USA
[2]Machine Learning Center Genoa (MalGa), Department of Civil, Chemical and Environmental Engineering (DICCA), University of Genoa, Via Montallegro 1, 16145 Genoa, Italy
[3]Department of Organismic and Evolutionary Biology and Museum of Comparative Zoology, Harvard University, Cambridge MA 02138 USA

[#]Correspondence: nbellono@harvard.edu, agnese.seminara@unige.it

Abstract

Jellyfish and sea anemones fire single-use, venom-covered barbs to immobilize prey or predators. We previously showed that the anemone *Nematostella vectensis* uses a specialized voltage-gated calcium (Ca_V) channel to trigger stinging in response to synergistic prey-derived chemicals and touch (Weir et al., 2020). Here we use experiments and theory to find that stinging behavior is suited to distinct ecological niches. We find that the burrowing anemone *Nematostella* uses uniquely strong Ca_V inactivation for precise control of predatory stinging. In contrast, the related anemone *Exaiptasia diaphana* inhabits exposed environments to support photosynthetic endosymbionts. Consistent with its niche, *Exaiptasia* indiscriminately stings for defense and expresses a Ca_V splice variant that confers weak inactivation. Chimeric analyses reveal that $Ca_V\beta$ subunit adaptations regulate inactivation, suggesting an evolutionary tuning mechanism for stinging behavior. These findings demonstrate how functional specialization of ion channel structure contributes to distinct organismal behavior.

Introduction

Sea anemones, jellyfish, corals, and hydrozoans of the Cnidarian phylum use specialized cells called nematocytes to sting for predation or defense. Mechanical and chemical stimuli from prey or predators act synergistically on nematocytes to mediate rapid discharge of a toxin-covered barb from its nematocyst organelle (Holstein and Tardent, 1984; Watson and Mire-Thibodeaux, 1994; Babonis and Martindale, 2014). Nematocyst discharge requires calcium (Ca^{2+}) influx and, as a one-time use organelle, is tightly controlled to prevent energetically wasteful stinging to irrelevant stimuli (Lubbock et al., 1981; Gitter et al., 1994; Watson and Hessinger, 1994). We previously found that the starlet sea anemone *Nematostella vectensis* uses a uniquely adapted voltage-gated Ca^{2+} channel (Ca_V) to integrate simultaneously presented chemical and mechanical cues that elicit nematocyst discharge. *Nematostella* Ca_V exhibits unusually "strong" steady-state voltage-dependent inactivation at resting membrane voltages to reduce cellular excitability and prevent stinging behavior in response to extraneous, non-prey touch signals. Chimeric analyses of *Nematostella* and mammalian Ca_V showed that the auxiliary βsubunit ($Ca_V\beta$) is required and sufficient for low-voltage steady-state inactivation in *Nematostella* Ca_V channel complexes. Ca_V inactivation is relieved by hyperpolarization of the nematocyte membrane potential to very negative voltages through the effect of prey-derived chemosensory signals that are synaptically transmitted from sensory neurons. Upon relieving Ca_V inactivation, direct touch responses are amplified to trigger nematocyst discharge (Weir et al., 2020). Thus, single nematocytes integrate synergistic cues to elicit a

precise response, representing a unique cellular system to study how cells detect and transduce signals to produce discrete behavior.

While Ca_V-mediated sensory integration represents one mechanism by which nematocytes "decide" when to sting, the incredible diversity of cnidarian biology suggests that stinging behavior must be adapted to support the demands of different lifestyles. Cnidarian taxa occupy diverse environmental niches and endure specific metabolic demands, predatory challenges, and environmental pressures for survival, which results in distinct selective pressures on nematocyte evolution (Beckmann and Özbek, 2012; Babonis et al., 2022). *Nematostella vectensis* and *Exaiptasia diaphana* represent an example of closely related cnidarians with differing environmental niches and metabolic demands (Darling et al., 2005; Bedgood et al., 2020). *Nematostella* are found in shallow brackish water of coastal marshes where they are buried in the mud, hidden from predators, with only their tentacles exposed to catch unsuspecting passing prey (Fraune et al., 2016). Thus, we hypothesize that their stinging is under tight regulation adapted for opportunistic predation. In contrast, *Exaiptasia* are exposed to predators while living in shallow, open ocean environments that provide sufficient sunlight for their endosymbionts to produce important photosynthetic products and nutrients (Baumgarten et al., 2015). Considering these dramatically different ecological contexts, we hypothesized that Ca_V-mediated regulation of nematocyte discharge has adapted to reflect the demands on stinging behavior in these two anemones. We therefore probed the behavior of these related but distinct anemones and investigated how subtle tuning of a shared molecular-regulatory mechanism drives adaptation in physiology and behavior associated with niche diversification.

In this study, we find that the symbiotic anemone *Exaiptasia* stings in response to mechanical stimuli alone, independent of predation pressure. This behavior serves as a stark contrast with *Nematostella* stinging, which is only elicited by synergistic prey chemicals and touch. Markov decision process modeling coupled with behavioral experiments revealed that *Nematostella* stings as an optimal predator, whereas *Exaiptasia* exhibits optimal defensive stinging behavior. Consistent with indiscriminate stinging behavior, we discover that *Exaiptasia* nematocyte physiology lacks the unusual Ca_V inactivation used by *Nematostella* to inactivate cells at rest and prevent responses to touch in the absence of prey chemicals. "Weak" steady-state inactivation of *Exaiptasia* Ca_V is mediated by a splice isoform of the beta subunit ($Ca_V\beta$) with a distinct N-terminus and allows for robust activation from resting membrane potentials. Analysis of chimeric jellyfish and anemone channels reveals that Ca_V inactivation is broadly regulated by the $Ca_V\beta$ N-terminus, suggesting an evolutionary tuning mechanism that could contribute to specific stinging behavior across cnidarians. Thus, we propose Ca_V adaptations as one molecular mechanism that could shift predatory versus defensive stinging in cnidarians. These results highlight how subtle adaptations in protein structure contribute to complex organismal behavior.

Results

Comparative sea anemone stinging behavior

In their natural habitat, *Nematostella* are hidden by burrowing within the sandy substrate and use an opportunistic predatory strategy to capture prey with their tentacles. In contrast, symbiotic *Exaiptasia* are found within open waters where they experience greater risk of predation and therefore must adopt a more defensive stance. Thus, we first asked whether differences in ecological pressure are reflected by stinging behavior. Consistent with our previous findings, we observed *Nematostella* stinging in response to simultaneously delivered prey extract and touch, reflecting stinging control adapted for predation (**Figure 1**) (Weir et al., 2020). Strikingly, *Exaiptasia* tentacles instead exhibited robust stinging even in the absence of prey chemicals (touch alone, **Figure 1**). Similar touch-evoked stinging was observed for *Exaiptasia* acontia, which are defensive nematocyte-enriched structures that are ejected and release toxins to repel

predators (Lam et al., 2017). Considering the drastic differences in stinging behavior, we wondered if *Exaiptasia*'s indiscriminate stinging reflects a distinct control strategy.

To investigate whether different stinging behaviors might be suited for predation versus defense, we developed a normative theory aimed at predicting optimal stinging behavior as a function of nutritional state (see ***Supplementary Information*** for model details). We focused on stinging intensity, defined as the fraction of nematocysts discharged during a stinging event, and asked whether nutritional state would affect optimal predatory and defensive stinging. In the language of decision models, the intensity of stinging is an action, and it is chosen by the agent, or anemone. In our study, "choice" of stinging means modulation of behavior with nutritional state, rather than a cognitive process. Each choice has associated costs and benefits that depend on the environment. Because anemones sting many times over the course of their lives, an optimal behavior must account for overall costs and benefits after many events; therefore, this is a sequential decision-making problem.

We modeled the optimal stinging response to a given environment by using Markov decision processes (MDP). Each anemone was modeled as an "agent" that must hedge the intensity of its stinging response. The environment, including the identity of prey, predators, and the physiological state of the animals, defines the likelihood, costs, and benefits of successful stinging. Specifically, intense stinging responses are costly since each fired nematocyst needs to be regenerated. But they are also more likely to succeed because greater discharge of stinging barbs increases the likelihood of contact and envenomation. The cost per nematocyte was first assumed to be constant and equivalent for defensive and predatory stinging as nematocyst discharge requires regeneration in either case (**Figure 2A,** solid line, filled circles). We assumed that the benefits of successful predatory stinging depend on the capture and consumption of prey, which improves satiation (**Figure 2B left**). In contrast, stinging a predator for defense would not improve nutritional state, hence the benefits of stinging would not depend on starvation (**Figure 2C left**). We then used the model to predict optimal stinging that maximizes the sum of all future benefits while minimizing costs during starvation (i.e. maximizing the value function, see Materials and Methods). We then tested the prediction directly against experiments with behaving animals.

Using this approach, we found that optimal stinging strategies were completely different for predatory versus defensive behavior. Regardless of the specific environment (likelihood to succeed and specific costs and benefits), predatory stinging increased with starvation (**Figure 2B, right** solid lines, filled circles**).** To test our theory regarding predatory stinging, we carried out simulations in which agents discharged a random fraction of nematocytes between 0 and 1, regardless of starvation. Random stinging was unsustainable over numerous events and agents quickly reached maximal starvation state. Agents using optimal predatory stinging discharged more nematocysts when starved and less when satiated, leading to sustained stinging behavior and survival. This was true even if they fired the same fraction of nematocytes as the random agent (**Figure 2D**). In contrast, optimal stinging for defense stayed constant with starvation (**Figure 2B, right** solid lines, filled circles). Importantly, while the precise optimal response depended on the details of cost and reward that defined the MDP, the differences between increasing predatory stinging versus unchanging defensive stinging were consistent and largely independent of assumptions associated with each reward function (further described in **Supplementary Information**). These results reflect greater rewards to predatory anemones upon stinging during starvation, whereas defensive anemones sting at a similar rate regardless of nutritional status. Thus, our model predicts robust differences in predatory versus defensive stinging behavior.

We next sought to experimentally test whether pressure to predate regulates stinging in *Nematostella* and *Exaiptasia*. To do so, we fed both species of anemones copious amounts of prey (brine shrimp, *Artemia*

143 *nauplii*) for 1-2 weeks and then deprived them of food for 5 days. Following manipulation of prey availability,
144 *Nematostella* significantly increased stinging in response to starvation, while *Exaiptasia* stinging remained
145 relatively constant despite complete deprivation of prey (**Figure 2E**, symbols with error bars). The behavior
146 was remarkably consistent with our normative theory of optimal stinging strategies for predation versus
147 defense (**Figure 2E,** filled circles). Furthermore, changes in *Nematostella* and *Exaiptasia* stinging were not
148 due to changes in the abundance of nematocytes because tentacles from both animals were abundantly
149 armed with nematocytes across feeding conditions (**Figure 2S1A**). The experimental behavior of
150 *Exaiptasia* showed a slight decrease in stinging with starvation. To account for this decrease we revisited
151 the theory and assumed that the cost per nematocyte slightly increased with starvation (**Figure 2A,** dashed
152 lines and open circles). In this case, the optimal response slightly decreased for defensive stinging but
153 increased for predatory stinging (**Figure 2B right** open circles and **Figure 2C right,** dashed lines, open
154 circles). In fact, the fit between theory and data for both *Nematostella* and *Exaiptasia* improved when the
155 cost increased slightly with starvation (**Figure 2E**, open circles). The more dramatic and less realistic
156 increase of the cost with starvation is discussed in the Supplementary Information and may lead to a
157 decrease in predatory stinging. Thus, we conclude that *Nematostella* controls stinging for opportunistic
158 predation while *Exaiptasia* stinging is indiscriminate and serves a greater defensive role for this symbiotic
159 anemone.
160
161 *Sea anemones with different stinging behavior use distinct Ca_V channels*
162 We next probed the physiological basis underlying these significantly different stinging behaviors. We
163 previously found that *Nematostella* stinging is triggered by a specialized Ca_V channel that exhibits strong
164 inactivation at negative voltages to prevent responses to extraneous non-prey mechanical stimuli (Weir et
165 al., 2020). Ca^{2+} influx triggers an increase in hydrostatic pressure inside the nematocyst capsule that forces
166 the stinging thread to evert explosively at an acceleration of up to 5.41×10^6g, placing it among the fastest
167 biological processes in existence (Lubbock and Amos, 1981; Lubbock et al., 1981; Holstein and Tardent,
168 1984; Weber, 1990; Gitter et al., 1994; Tardent, 1995; Nüchter et al., 2006). Similar to *Nematostella*,
169 *Exaiptasia* stinging required extracellular Ca^{2+} and was abolished by Cd^{2+}, a Ca_V channel blocker (**Figure**
170 **3A**). Consistent with a Ca^{2+}-dependent stinging mechanism, whole-cell patch clamp recordings from
171 nematocytes revealed the presence of voltage-gated inward currents that were blocked by Cd^{2+},
172 suggesting that *Exaiptasia* nematocytes also use Ca_V channels to control stinging (**Figure 3B**). Indeed,
173 Ca_V currents in *Exaiptasia* nematocytes exhibited similar voltage-dependent activation properties
174 compared with *Nematostella* nematocytes (**Figure 3C**). Thus, in agreement with previous findings, we
175 conclude that Ca^{2+} influx via Ca_V channels is broadly important for stinging.
176
177 Ca_V channels respond to positive membrane potentials by opening to conduct Ca^{2+}. However, sustained
178 positive voltage drives Ca_Vs to transition to a non-conducting state (inactivation) that prevents re-activation
179 until channels return to a resting state induced by negative membrane potentials. In most cells, voltage-
180 gated ion channel inactivation prevents extended responses to repetitive or prolonged stimulation.
181 *Nematostella* Ca_V, is unusual because it inactivates at very negative voltages to prevent responses from
182 resting potential, resulting in nematocytes that cannot fire from rest (Weir et al., 2020). In contrast to
183 *Nematostella* nematocytes in which half of all Ca_V channels ($V_{i1/2}$) were inactivated at ~ -93mV, *Exaiptasia*
184 nematocytes exhibited two distinct inactivation phenotypes: (1) nematocytes with low-voltage threshold
185 (low-V) inactivation similar to that of *Nematostella* (low-V, $V_{i1/2}$ = ~ -85mV); and (2) a distinct population
186 with weak, high-voltage (high-V) threshold inactivation similar to its well-characterized mammalian
187 orthologue (high-V, $V_{i1/2}$ = ~ -48mV) (**Figure 3D**). While we did not observe a correlation with abundance
188 or distinct cellular morphology (Östman, 2000; Kass-Simon and Scappaticci, 2002; Grajales and
189 Rodríguez, 2014), we could clearly distinguish the two populations based on these electrophysiological
190 features. Importantly, high-V nematocyte inactivation was minimal at resting voltages (~ -70mV), so nearly

all channels would be available to amplify depolarizing signals, such as those elicited by touch. Thus, these markedly different physiological properties correlate with distinct stinging behavior: *Nematostella* uses unusual low-voltage Ca_V inactivation to integrate sensory cues for tightly regulated predatory stinging. In contrast, *Exaiptasia* employs a population of nematocytes with weak Ca_V inactivation, consistent with direct activation from resting potentials and stinging to touch alone.

What is the molecular basis of distinct nematocyte physiology? Ca_V channels are made of at least three subunits: the pore-forming α and auxiliary β and α2δ subunits. Transcriptomics revealed that nematocyte-enriched tentacles of *Exaiptasia* expressed *cacna1a*, the pore-forming subunit homologous to that of the previously characterized *Nematostella* nematocyte Ca_V channel (**Figure 4S1**). We also analyzed the Ca_V β subunit, $Ca_V\beta$, which is required and sufficient for the unusual inactivation properties observed in *Nematostella* Ca_V (Weir et al., 2020) (**Figure 4S1**). From *Exaiptasia*, we identified two isoforms of $Ca_V\beta$: $EdCa_V\beta1$ and $EdCa_V\beta2$. Droplet digital PCR assays of mRNA abundance showed that both isoforms are expressed throughout *Exaiptasia* tissues, suggesting they could both be functionally important (**Figure 4A, 4S1B**). To localize $Ca_V\beta$, we used *in situ* hybridization to determine that distinct nematocyte populations expressed either $EdCa_V\beta1$ or $EdCa_V\beta2$ mRNA (but not both) in the same cell (**Figure 4B**).

Considering this expression profile, we wondered if the two $Ca_V\beta$ isoforms could mediate low-V and high-V inactivation phenotypes in *Exaiptasia* nematocytes. To investigate this question, we heterologously expressed each β subunit isoform with other well-characterized Ca_V subunits (mammalian Ca_V α and α2δ) that express well in heterologous systems. Both channels exhibited functional Ca_V currents with similar activation thresholds (**Figure 4C**). However, $EdCa_V\beta1$- and $EdCa_V\beta2$-containing channels significantly differed in their inactivation properties. $EdCa_V\beta1$ inactivated at negative voltages, similar to channels containing *Nematostella* $Ca_V\beta$ ($NveCa_V\beta$). In contrast, $EdCa_V\beta2$ mediated Ca_V currents with weak inactivation, more like channels containing rat $Ca_V\beta2a$ (**Figure 4C, D**). Thus, $EdCa_V\beta1$ and $EdCa_V\beta2$ confer strong, low-voltage and weak, high-voltage steady-state inactivation, respectively, and are expressed in distinct nematocytes, consistent with low-V and high-V threshold inactivating nematocyte populations. Genomic alignment revealed that alternative splicing at the N-terminus gives rise to $EdCa_V\beta1$ and $EdCa_V\beta2$ isoforms, serving as a mechanism to dynamically tune nematocyte physiology and potentially stinging behavior in contrast to adaptation through gene duplication and divergence (**Figure 4E**). Furthermore, by expressing two functional variants, *Exaiptasia* could use distinct nematocyte populations for different behaviors, including a less pronounced role for predation.

Structural adaptations across cnidarian Ca_V channels

We next asked how variation in $Ca_V\beta$ structure mediates strong phenotypes by testing whether distinct protein domains confer low or high voltage-dependent inactivation. We first compared rat rCavβ2a and *Nematostella* $NveCa_V\beta$, which have significantly different voltage-dependent properties (Weir et al., 2020). Swapping the well-characterized SH3, HOOK, and GK domains had no effect on inactivation, but the $NveCa_V\beta$ N-terminus was both required and sufficient for low voltage-dependent inactivation (**Figure 5A, B**). Indeed, swapping only the N-terminus of $NveCa_V\beta$ was sufficient to shift rat rCavβ2a-conferred inactivation by ~ -75mV (**Figure 5A, B**). This finding is consistent with the variation in $EdCa_V\beta$ splice isoforms, in which differences in the N-terminus account for a ~ 40mV difference in inactivation thresholds.

To explore evolutionary relationships of $Ca_V\beta$, we constructed a phylogenetic tree of sequences from various cnidarians including *Nematostella vectensis* (anemone, $NveCa_V\beta$), *Exaiptasia diaphana* (anemone, $EdCa_V\beta1$ and $EdCa_V\beta2$), *Cyanea capillata* (jellyfish, $CcCa_V\beta$), *Physalia physalis* (hydrozoan, $PpCa_V\beta$), *Clytia hemisphaerica* (jellyfish, $ChCa_V\beta$), *Cassiopea xamachana* (jellyfish, $CxCa_V\beta$), and the Rat β subunit (rCavβ2a) as an outgroup (**Figure 5C**). Sequence comparison across all amino acid positions

revealed that the N-terminus exhibited the greatest sequence diversity (**Figure 5D**), consistent with previous findings showing extensive alternative splicing in this region in other organisms (Helton and Horne, 2002; Helton et al., 2002; Takahashi et al., 2003; Foell et al., 2004; Vendel et al., 2006; Ebert et al., 2008; Buraei and Yang, 2010; Siller et al., 2022). We found that all cnidarian $Ca_V\beta$s conferred voltage-gated currents when co-expressed with $Ca_V\alpha$ and α2δ subunits and had relatively low voltage thresholds for inactivation compared with rCavβ2a or $EdCa_V\beta2$ (**Figure 5E, 5S1A, 5S1B**). Importantly, swapping the N-termini of each cnidarian $Ca_V\beta$ onto $EdCa_V\beta2$ was sufficient to shift voltage-dependent inactivation to more negative values (**Figure 5E, 5S1C**). Thus, alternative splicing at the N-terminus could serve as a broad molecular mechanism for tuning Ca_V function. Collectively, these findings substantiate the importance of $Ca_V\beta$ in modulating inactivation and suggest a mechanism that could dynamically regulate a small region of only one subunit in the Ca_V protein complex to tune complex stinging behavior.

Discussion

Collectively, our studies on cnidarian stinging, here and (Weir et al., 2020), reveal different behavior in the primarily predatory anemone *Nematostella* versus the symbiotic anemone *Exaiptasia*. This study used a combination of theory and experimentation to uncover the molecular basis of regulation of the divergent behavior of *Exaiptasia* that uses stinging primarily for defense. Indeed, *Exaiptasia* obtains a large fraction of its energy and nutrients from endosymbiotic algae (Muscatine et al., 1981; Shick and Dykens, 1984; Steen, 1988), thus reducing overall pressure to predate. This finding is consistent with a common ecological theme in which symbiotic relationships are established whereby one partner provides food and the other provides shelter and defense (Lehnert et al., 2012; Bucher et al., 2016). Therefore, it is plausible that synergistic selection drives higher investment in defensive structures to protect symbiotic species.

Our results demonstrate that molecular adaptations tune distinct stinging behavior: *Nematostella* $Ca_V\beta$ confers an unusually low threshold for inactivation, basally inhibiting nematocytes unless they are exposed to synergistic prey cues: chemical (hyperpolarizing to relieve inactivation) and mechanical (depolarizing to recruit available Ca_V channels and elicit stinging) (Weir et al., 2020). These physiological mechanisms reflect a stinging strategy suited to opportunistic predation by *Nematostella*, which burrow within shallow marshes and sting unsuspecting prey. Consistent with the predictions of optimal control theory, *Nematostella* increased stinging with starvation, suggesting that evolution has shaped its stinging response to maximize benefits for predation. In contrast, *Exaiptasia* nematocytes contain a functionally specialized splice variant of $Ca_V\beta$ to mediate high threshold voltage-dependent Ca_V inactivation, consistent with Ca_V channel availability to amplify depolarizing signals from rest and stinging in response to touch alone. Thus, *Exaiptasia* physiology is consistent with an indiscriminate stinging strategy for defense, necessary for survival in an exposed environment that facilitates endosymbiotic photosynthesis (Muscatine et al., 1981; Shick and Dykens, 1984; Steen, 1988). Such stinging behavior is likely synergistic with physical escape for some cnidarians (Pallasdies et al., 2019; Wang et al., 2023). Consistent with the predictions of optimal control theory, *Exaiptasia* stinging was nearly independent of starvation, suggesting that evolution has shaped the stinging response to maximize benefits for defense. Using molecular information gleaned from analyzing these two cnidarians, we find that $Ca_V\beta$ variation across cnidarians mediates differences in voltage-dependent inactivation, which could contribute to differences in stinging behavior. Thus, our study provides an example by which alternative splicing could account for adaptation across this diverse plethora of organisms and habitats.

While theory predicts robust trends for optimal predation and defense independent of environment, the precise nature of the predicted behavior does depend on the environment. In vivo, stinging is likely influenced by stimulus identity and intensity, background turbulence, and other factors. For example, cnidarians may have evolved distinct innate responses for different prey and use chemical sensing to enact

the appropriate stinging response. In this case, optimal control theory can be used to predict the optimal response to known salient environmental cues. Alternatively, cnidarians may learn that specific prey are palatable and easy to catch through repeated exposure (Botton-Amiot et al., 2023). In this example, optimal control theory must be replaced by reinforcement learning as the likelihood of successful predation and its cost and benefits (the environment) are unknown (Sutton and Barto, 2018).

Indeed, stinging is a complex process mediated by numerous molecular components and cell types that could be subject to evolutionary change or acute modulation. Cnidarians occupy diverse ecological niches and experience varying metabolic demands, predatory challenges, and other survival pressures that could influence stinging behavior. Beyond cnidarians with stationary lifestyles that support photosynthetic endosymbionts (symbiotic anemones, corals, sea pens) and those that use opportunistic “sit-and-wait” ambush predatory strategies (burrowing anemones, siphonophores), others have evolved mobile lifestyles to actively capture prey (jellyfish) (Muscatine et al., 1981; Shick and Dykens, 1984; Steen, 1988; Fraune et al., 2016; Damian-Serrano et al., 2022). Stinging by mobile cnidarians could be subject to different physical demands, such as mechanical disturbance from increased turbulence that could necessitate distinct molecular control. Furthermore, stinging can be influenced by acute factors such as physiological state and various sensory cues, including chemicals, touch, or light (Pantin, 1942; Giebel et al., 1988; Thorington and Hessinger, 1988; Watson and Hessinger, 1989; Plachetzki et al., 2012; Ozment et al., 2021; Aguilar-Camacho et al., 2023). Thus, further inquiry into modulation of stinging across physiological states such as nutritional condition, altered symbiotic relationships, or developmental stages (Sandberg et al., 1971; Columbus-Shenkar et al., 2018) could reveal dynamic regulation by synaptic connections, hormones, or modulation of transcriptional or translational programs (Westfall et al., 1998, 2002; Westfall, 2004; Weir et al., 2020). Importantly, across all these scenarios, nematocytes remain single-use cells, so it is essential that signaling cascades control discharge in response to the most salient environmental stimuli.

As an early-branching metazoan lineage and sister group to Bilateria (Cartwright et al., 2007), cnidarians are a useful model for probing origins of the nervous system and behavioral specialization (Steele et al., 2011, Jékely et al., 2015; Pallasdies et al., 2019). Here we present a comparative approach across related cnidarians with distinct physiology and ecology to suggest that behavioral complexity emerges from subtle tuning of single proteins, even in non-neuronal cells. Indeed, cnidarians pose a unique opportunity for the integrative exploration of the evolution of animal behavior. Even beyond neural computations, the emergence of novel cell types among diverse cnidarian body plans, sophisticated predator-prey interactions, and symbioses all contribute to biological novelty and niche expansion (Technau and Steele, 2012). Overall, this work demonstrates how studying evolutionary novelties like stinging behavior can yield broad insight into signal transduction, cellular decision making, and suggests that the evolution of behavior must be examined across all tiers of biological organization.

Materials and Methods

Animals and Cells

Starlet sea anemones (*Nematostella vectensis*) were provided by the Marine Biological Laboratory (Woods Hole, Massachusetts). Adult animals of both sexes were used and kept on a 14 hr light/10 hr dark cycle at 26°C in 1/3 natural sea water (NSW). *Exaiptasia spp.* were purchased through Carolina Biological Supply Company (Cat #162865). Adult animals of both sexes were used following being kept on either a 10 hr light/14 hr dark cycle at 26°C in natural sea water (NSW) or a 14 hr light/10 hr dark cycle at 26°C in natural sea water (NSW). *Cassiopea spp.* were purchased through Carolina Biological Supply Company (Cat #162936). Unless stated otherwise, all animals were fed freshly hatched brine shrimp (Artemia) twice a week.

Exaiptasia diaphana were bleached through chemical methods (menthol-induced). Menthol (100mM in 100% ethanol; Sigma-Aldrich) was added to NSW at a final concentration of 0.2mM (Matthews et al., 2016). The anemones were incubated in the menthol/NSW treatment solution for a maximum of 8hr per day and outside of treatments anemones were incubated in NSW. For 2 weeks, anemones were treated 4 days per week and kept in the dark continuously starting from day 1 of treatment, aside from treatment changes. Animals were fed with Artemia approximately twice per week between bleaching treatments, enabling successful bleaching with minimal mortality. Their symbiotic status was assessed via fluorescence microscopy at the end of each week. For starvation experiments, animals were fed to excess for 1-2 weeks before the trial and withheld food entirely during the trial period and given water changes twice a week.

Nematostella nematocytes were isolated from tentacle tissue, which was harvested by anesthetizing animals in high magnesium solution containing (mM): 140 NaCl, 3.3 Glucose, 3.3 KCl, 3.3 HEPES, 40 $MgCl_2$. Cells were isolated from tentacles immediately prior to electrophysiology experiments by treatment with 0.05% Trypsin at 37°C for 15-20 min and mechanical dissociation in divalent free recording solution (mM): 140 NaCl, 3.3 Glucose, 3.3 KCl, 3.3 HEPES, pH 7.6. Dissociated cells were held on ice until use. Basitrichous isorhiza nematocytes were isolated from tentacles and identified by the presence of a capsule with high refractive index containing a barbed thread, oblong shape, and the presence of a cnidocil. *Exaiptasia* nematocytes were isolated from tentacle tissue immediately prior to electrophysiology experiments by incubation in a heat shock dissociation solution with (in mM): 430 NaCl, 10 KCl, 150 sucrose, 5 NaEGTA, 10 HEPES, 10 glucose, pH 7.6 at 45°C for 15-20 min and mechanical dissociation in the same solution. Dissociated cells were held on ice until use. Nematocytes were isolated from tentacles and identified by the presence of a capsule with high refractive index, oblong shape, and the presence of one or multiple apical cilia.

HEK293T cells (ATCC) were grown in Dulbecco's Modified Eagle Medium (DMEM) (Gibco) supplemented with 10% fetal calf serum (Gibco) and 50 I.U./mL penicillin and 50 µg/mL streptomycin (Gibco) at 37°C, 5% CO2 using standard techniques. For transfection, HEK293 cells were washed with Opti-MEM Reduced Serum Media (Gibco) and transfected using lipofectamine 2000 (Invitrogen/Life Technologies Cat #11668019) according to the manufacturer's protocol. 1 µg each of *M. musculus* (mouse) *cacna1a* and rat *cacna2d1* and one of a wide variety of beta subunits (*Nematostella vectensis cacnb2.1* (NveCa$_V$β)*, Rattus norvegicus* (rat) *cacnb2a* (rCa$_V$β2a)*, Exaiptasia diaphana* Ca$_V$βs (EdCa$_V$β1, EdCa$_V$β2), *Cyanea capillata* Ca$_V$β (CcCa$_V$β), *Physalia physalis* Ca$_V$β (PpCa$_V$β), *Clytia hemisphaerica* Ca$_V$β (ChCa$_V$β), *Cassiopea xamachana* Ca$_V$β (CxCa$_V$β2)) were coexpressed with 0.5 µg eGFP. We also assayed an array of different EdCa$_V$β2 mutants with N-termini from different animals by coexpressing 0.5 µg eGFP, 1 µg of *M. musculus* (mouse) *cacna1a* and rat *cacna2d1,* and one of a variety of beta subunits (*Nematostella vectensis*

cacnb2.1 mutant (NveCa$_V$β-N)*, R. norvegicus* (rat) *cacnb2a* mutant (rCa$_V$β-N)*, Exaiptasia diaphana* Ca$_V$β mutants (EdCa$_V$β1-N, EdCa$_V$β2-N), *Cyanea capillata* Ca$_V$β mutant (CcCa$_V$β-N), *Physalia physali*s Ca$_V$β mutant (PpCa$_V$β-N), *Clytia hemisphaerica* Ca$_V$β mutant (ChCa$_V$β-N), *Cassiopea xamachana* Ca$_V$β mutant (CxCa$_V$β2-N)). To enhance channel expression, cells were incubated with transfection mix containing plasmid DNA and Lipofectamine 2000 in Opti-MEM for 6 hr at 37°C. Cell were then re-plated on coverslips, incubated for 1-2 hr at 37 °C, and then incubated at 30°C for 2-6 days before experiments. Rat *cacna2d1 (*RRID: Addgene_26575) and *cacna1a* were gifts from D. Lipscombe (RRID: Addgene_26578) and *cacnb2a* was a gift from A. Dolphin (RRID: Addgene_107424).

Molecular biology

RNA was prepared from tentacles, body, and acontia tissues of WT and bleached adult *Exaiptasia* using published methods (Stefanik et al., 2013). Each tissue was homogenized (Millipore Sigma Cat #Z359971) and RNA was extracted using TRIzol Reagent (Thermo Fisher Cat #15596026), then after skipping the salt precipitation steps, RNA was purified and concentrated with the RNA Clean & Concentrator-5 kit (Zymo Research). For ddPCR experiments, droplet generation (QX200™ Droplet Generator BioRad Cat #1864002) and transfer of droplets to ddPCR™ 96-Well Plates (Bio-Rad Cat #12001925) were performed according to manufacturer's instructions (Instruction Manual, QX200™ Droplet Generator – Bio-Rad). Custom primers and probes and One-Step RT-ddPCR Advanced Kit for Probes (Bio-Rad Cat #1864021) reaction reagents and Droplet Generation Oil for Probes (Bio-Rad Cat #1863005) were sourced from Bio-Rad (see Key Resources Table for primer and probe sequences). The ddPCR plate was sealed with a Pierceable Foil Heat Seal (Bio-Rad Cat #1814040) and the PX1™ PCR Plate Sealer (Bio-Rad Cat #1814000). Plates were transferred to a Bio-Rad Thermalcycler C1000 (Bio-Rad Cat #1851197). The cycling protocol was the following: 45°C reverse transcription step for 60 minutes, 95°C enzyme activation step for 10 minutes followed by 40 cycles of a two-step cycling protocol (denaturation step of 95°C for 30 seconds and annealing/extension step of 58°C for 1 minute), 98°C enzyme deactivation step for 10 minutes, and holding at 12°C for an indefinite period before transfer to the QX200 Droplet Generator. The plates were read with the Bio-Rad QX200 Droplet Generator & Reader (Cat #1864003) and the RNA concentration per sample was processed using QuantaSoft (Bio-Rad Cat #1864011). Data were exported to Microsoft Excel and Prism (Graphpad) for further statistical analysis.

Most plasmids, including *Nematostella vectensis cacnb2.1* (NveCa$_V$β)*, Exaiptasia diaphana* Ca$_V$βs (EdCa$_V$β1, EdCa$_V$β2), *Cyanea capillata* Ca$_V$β (CcCa$_V$β), *Physalia physali*s Ca$_V$β (PpCa$_V$β), *Clytia hemisphaerica* Ca$_V$β (ChCa$_V$β), *Cassiopea xamachana* Ca$_V$β (CxCa$_V$β2)), *Nematostella vectensis cacnb2.1* mutant (NveCa$_V$β-N)*, R. norvegicus* (rat) *cacnb2a* mutant (rCa$_V$β-N)*, Exaiptasia diaphana* Ca$_V$β mutants (EdCa$_V$β1-N, EdCa$_V$β2-N), *Cyanea capillata* Ca$_V$β mutant (CcCa$_V$β-N), *Physalia physali*s Ca$_V$β mutant (PpCa$_V$β-N), *Clytia hemisphaerica* Ca$_V$β mutant (ChCa$_V$β-N), *Cassiopea xamachana* Ca$_V$β mutant (CxCa$_V$β2-N), were synthesized by Genscript (Piscataway, NJ). Sequence alignments were carried out using Clustal Omega. Wild type and Chimeric Ca$_V$β sequences are listed in **Supplemental Table 1**.

Cnidarian beta sequences were obtained from RNA sequencing or NCBI: *Nematostella vectensis cacnb2.1* (NveCa$_V$β) sequence (Weir et al., 2020), *Exaiptasia diaphana* Ca$_V$βs from RNA sequencing and confirmation from NCBI accession number KXJ28099.1 (EdCa$_V$β1) and NCBI accession number XP_020893045.1 (EdCa$_V$β2), *Cyanea capillata* Ca$_V$β (CcCa$_V$β) from NCBI accession number AAB87751.1 (Jeziorski et al., 1998), *Physalia physali*s Ca$_V$β (PpCa$_V$β) from NCBI accession number ABD59026 (Bouchard et al., 2006), *Clytia hemisphaerica* Ca$_V$β (ChCa$_V$β) from the MARIMBA database (Leclère et al., 2019), *Cassiopea xamachana* Ca$_V$β (CxCa$_V$β2) from RNA sequencing as TRINITY_DN5778_c3_g1_i5.p1.

Transcriptomics

419 *Exaiptasia* were anesthetized in 15% $MgCl_2$ NSW solution in a dish surrounded by an ice bath for 15
420 minutes. Tentacle, body, and acontia tissue were dissected and flash frozen in the presence of liquid
421 nitrogen. *Cassiopea xamachana* were anesthetized in 10% $MgCl_2$ NSW solution in a dish surrounded by
422 an ice bath for 15-20 minutes. Oral arms, bell, and cassiosome tissues were dissected and flash frozen in
423 the presence of liquid nitrogen. All tissues were stored at -80°C until RNA extraction, library preparation,
424 and RNA sequencing was performed by Genewiz (Azenta) using a HiSeq (2x150 bp) platform. Reads were
425 examined for base quality distribution, kmer frequencies and adapter contamination by position in the read
426 using fastqc (The Babraham Institute Bioinformatics Group), then where relevant, Rcorrector was used to
427 remove erroneous k-mers (Song and Florea, 2015) and the FilterUncorrectablePEfastq python script from
428 the Harvard Informatics group was used to discard read pairs. TrimGalore (The Babraham Institute) was
429 then used to remove adapter contamination in reads and where relevant, Bowtie2 (Langmead and
430 Salzberg, 2012) was used to remove reads originating from rRNA and Trinity was used to assemble
431 reference transcriptomes *de novo* (Grabherr et al., 2011). Transdecoder was used to identify open reading
432 frames (Haas, BJ) and Diamond used to annotate the transcriptome (Buchfink et al., 2015). Reads were
433 pseudo-aligned and transcript abundance (TPM) was quantified using Kallisto (Bray et al., 2016) and our
434 novel transcriptome assemblies as a reference and visualization and alignments were performed with
435 Geneious Prime software and/or Clustal Omega (Madeira et al., 2022).
436
437 *Electrophysiology*
438 Recordings were carried out at room temperature using a MultiClamp 700B amplifier (Axon Instruments)
439 and digitized using a Digidata 1550B (Axon Instruments) interface and pClamp software (Axon
440 Instruments). Whole-cell recording data were filtered at 1kHz and sampled at 10kHz. Ca_V activation data
441 were leak-subtracted online using a p/4 protocol, and all membrane potentials were corrected for liquid
442 junction potentials.
443
444 For whole-cell nematocyte recordings, borosilicate glass pipettes were polished to 8-10MΩ for
445 *Nematostella* and 4-6MΩ for *Exaiptasia*, respectively. The standard *Nematostella* medium was used as
446 the extracellular solution and contained (in mM): 140 NaCl, 3.3 glucose, 3.3 KCl, 3.3 HEPES, 2 $CaCl_2$, 0.5
447 $MgCl_2$, pH 7.6, 260-280mOsm. The standard *Exaiptasia* medium was used as extracellular solution and
448 contained (in mM): 430 NaCl, 10 KCl, 10 $CaCl_2$, 50 $MgCl_2$, 10 HEPES, pH 7.6, 800-900mOsm. The
449 intracellular solution for both *Nematostella* and *Exaiptasia* contained (in mM): isolating inward currents (in
450 mM): 500 cesium methanesulfonate, 4 $MgCl_2$, 10 CsEGTA, 10 HEPES, 30 sucrose, pH 7.6, 260-280mOsm
451 for *Nematostella* and 800-900mOsm for *Exaiptasia*. For *Nematostella* nematocyte recordings, voltage-
452 dependent inactivation was measured during a 200ms activating pulse of -20mV following a series of 1s
453 pre-pulses ranging from -110mV to 30mV, holding at -110mV. Voltage-gated currents were measured
454 through a series of 200ms voltage pulses in 10mV increments from -110mV to 70mV, holding at -110mV.
455 For *Exaiptasia* nematocyte recordings, voltage-dependent inactivation was measured during a 200ms
456 activating pulse of 0mV following a series of 1s pre-pulses ranging from -110mV to 30mV, holding at -
457 110mV. For both *Nematostella* and *Exaiptasia,* voltage-gated currents were measured through a series of
458 200ms steps 200ms voltage pulses in 10mV increments from -110mV to 70mV, holding at -110mV. For
459 Cd^{2+} experiments, 500µM Cd^{2+} (dissolved in water) was applied locally and voltage-dependent activation
460 was assessed through a single 200ms step to 0mV from a holding potential of -110mV.
461
462 For whole-cell recordings in HEK293 cells, pipettes were 3-6MΩ. The standard extracellular solution
463 contained (in mM): 140 NaCl, 5 KCl, 10 HEPES, 2 $CaCl_2$, 2 $MgCl_2$, 10 Glucose, pH 7.4, 300-310mOsm.
464 The intracellular solution contained (in mM): 5 NaCl, 140 cesium methanesulfonate, 1 $MgCl_2$, 10 EGTA,
465 10 HEPES, 10 sucrose, pH 7.2, 300-310mOsm. For Ca^{2+} currents in heterologously expressed channels,
466 voltage-dependent inactivation was measured in one of two ways: (1) during an activating pulse of 0mV

467 following a series of 1s pre-pulses ranging from -110mV to 50mV and holding potential of -80mV; or (2)
468 during an activating pulse of 0mV following a series of 1s pre-pulses ranging from -110mV to 80mV and
469 holding potential of -90mV. Voltage-gated Ca^{2+} currents were measured in response to 200ms voltage
470 pulses in 10mV increments from -130mV to 80mV with -110mV holding potential. Voltage-dependent
471 inactivation was quantified as I/I_{max}, with I_{max} occurring at the voltage pulse following a -110mV prepulse.
472 In some instances, inactivation curves could not be fitted with a Boltzmann equation and were instead
473 fitted with an exponential. G-V relationships were derived from I-V curves by calculating G: $G=I_{CaV}/(V_m-$
474 $E_{rev})$ and fit with a Boltzmann equation. Data was processed and analyzed in Clampfit (pClamp 11 Software
475 Suite, Molecular Devices) and Microsoft Excel and Prism (GraphPad).
476
477 *In situ hybridization (BaseScope)*
478 Adult *Exaiptasia* were paralyzed in anesthetic solution (15% $MgCl_2$), rinsed in PBS, then embedded in
479 Tissue-Tek O.C.T. Compound (Sakura Cat #4583) in cryomolds (Sakura Tissue-Tek® Cryomold®,
480 Intermediate, Cat #4566) and flash frozen on dry ice and stored at -80°C. Cryostat sections (18-20µm)
481 were adhered to Fisherbrand™ Superfrost™ Plus Microscope Slides (Fisher Scientific Cat #12-550-15)
482 and flash frozen on dry ice and stored at -80°C until used for BaseScope. The BaseScope Duplex Detection
483 Reagent Kit (Advanced Cell Diagnostics Cat #323800) and the manufacturer's manual (BaseScope Duplex
484 Detection Reagent User Manual, ACDBio) was followed to hybridize custom probes or positive control (Cat
485 #700101) or negative control probes (Cat #700141) to targets in tissue cryosections and amplify signals.
486 Samples were imaged on an Olympus BX41 Phase Contrast & Darkfield Microscope (Olympus Cat #BX41-
487 PH-B) and images were acquired using the Olympus CellSens software and Olympus DP25 5MP Color
488 Firewire Camera.
489
490 *Behavior*
491 Discharge of nematocysts was assessed based on well-established assays (Gitter et al., 1994; Watson
492 and Hessinger, 1994; Weir et al., 2020). For assaying discharge, 5 mm round coverslips were coated with
493 a solution of 25% gelatin (w/v) dissolved in NSW (for *Exaiptasia*) or 1/3 NSW (for *Nematostella*) and
494 allowed to cure 3-4 hr prior to use. Coverslips were presented to the animal's tentacles for 5 seconds and
495 then immediately imaged at 20X magnification using a transmitted light source. To assay behavioral
496 responses to prey-derived chemicals, freshly hatched brine shrimp were flash frozen and ground to a
497 powder with a mortar and pestle (Fisherbrand), then filtered through a 0.22µm syringe filter (VWR Cat
498 #28145-501) and osmolarity adjusted for the specific anemone species. Coverslips were submerged in
499 prey extract for 10 seconds then immediately presented to the animal. Nematocytes visualized on
500 coverslips were only those that embedded in the gelatin after discharge. For experiments using
501 pharmacological agents such as $CdCl_2$, coverslips were submerged in a solution of 1M (*Exaiptasia*) or
502 10mM (*Nematostella*) Cd^{2+} in milli-Q water for 10 seconds then immediately presented to the animal. After
503 performing the experiments, the animals were given several water changes to remove Cd^{2+}. Experiments
504 carried out in the absence of extracellular Ca^{2+} were nominally Ca^{2+} free and did not include use of
505 extracellular chelators. The region of the highest density of discharged nematocytes on the coverslip was
506 imaged at 20X. Images were acquired with MetaMorph Microscopy Automation and Image Analysis
507 Software (Molecular Devices) and the number of discharged nematocysts was counted by eye. Images
508 were processed in Fiji (ImageJ) (Schindelin et al., 2012). *Exaiptasia* and *Nematostella* tentacles were
509 examined by cutting a small portion of exposed tentacles and sandwiched between glass coverslips and
510 then imaged at 20X with the MetaMorph software.
511
512 *Phylogenetic and Genomic analyses*
513 To infer exon boundaries and isoforms, we aligned $EdCa_V\beta1$ (NCBI accession number LJWW01000015.1)
514 and $EdCa_V\beta2$ (NCBI accession number XM_021037386.2) to the *Exaiptasia diaphana* reference genome

(BioProject PRJNA261862) (Baumgarten et al., 2015) using GMAP version 2015-07-23 (Wu and Watanabe, 2005). For phylogenetic analyses, we aligned nucleotide sequences with MAFFT v.7 (Katoh and Standley, 2013). We used ModelFinder (Kalyaanamoorthy et al., 2017) to assess the best model of substitution for phylogenetic inference. We estimated a maximum likelihood gene tree in IQ-TREE v2.0 (Minh et al., 2020). Support for clades was calculated using ultrafast bootstrap approximation UFBoot2 (Hoang et al., 2018). Percentage of identity for amino acids was calculated in overlapping windows.

Mathematical model: Optimal control theory for the stinging response

To model *Nematostella,* we assume the agent stings for predation. We thus introduce the state of starvation, s, that ranges from 0 to 1; at $s = 0$ the agent is least starved and at $s = 1$ the agent is most starved. At each time step, the agent decides to perform an action (sting), a, representing the intensity of the attack; a ranges from 0 to 1, and is experimentally compared to the fraction of nematocytes fired in the behavioral assay. Each action has a cost that is proportional to the fraction of nematocysts that are fired, $c(a) = c_0 a$ where c_0 is the cost of discharging all nematocysts at once, or cost of full discharge, and we first consider c_0 constant. Each stinging event has a probability $p(a)$ of achieving successful predation, where $p(a)$ increases with a (more intense attacks are more costly and more likely to succeed). A successful attack leads to the transition to the next state s' where the agent is more satiated $s \to s' = s - 1$ whereas a failed attack leads to higher starvation state $s \to s' = s + 1$. The most starved state is absorbing, which is equivalent to a point of no return. A reward $r(s')$ is assigned to the state of starvation reached upon attack, indicating its desirability ($r(s')$ is a decreasing function of s'), and the most starved state entails a starvation penalty $r(1) < 0$. Without loss of generality, all costs and rewards are normalized to the penalty of starvation, hence penalty of starvation is $r(1) = -1$. Our goal is to choose actions that maximize the expected sum of all future net rewards (reward - cost) for each state, which is called the value function. As customary in infinite horizon problems, we ensure convergence of the value function by introducing an effective horizon, i.e. by discounting exponentially rewards that are further in the future with a discount rate $\gamma < 1$.

The optimal value of a state, $V^*(s)$ and the corresponding optimal action $a^*(s)$ are obtained by solving the Bellman Optimality equation (Bellman, 2003).

$$V^*(s) = \max_a \big(p(a)\big(r(s-1) - c(a) + \gamma V^*(s-1)\big) + (1 - p(a))(r(s+1) - c(a) + \gamma V^*(s+1)\big) \quad (1)$$

$$a^*(s) = \operatorname*{argmax}_a \big(p(a)\big(r(s-1) - c(a) + \gamma V^*(s-1)\big) + (1 - p(a))(r(s+1) - c(a) + \gamma V^*(s+1)\big)$$

With the boundary condition $V^*(1) = 0$. We solve these equations numerically with the value iteration algorithm (Sutton and Barto, 2018) and analytically under the assumption that $a^*(s)$ varies slowly with s (details of the asymptotic method can be found in ***Supplementary Information***). The asymptotic solution reproduces well the numerical results (compare lines and full circles in **Figure 2B right**, where we used $c_0 = 1$ and $p = p_M(2 - a^2)$ and $p_M = 0.8$ and showcased two different functional forms for *r(s)*, $r(s) = 10\, tan^{-1}\,(1 - s)$; $r(s) = 5\, cos\left(\frac{s\pi}{2}\right)$). We also explored how well the asymptotic result can capture the trend of the numerical result by varying the parameters in these three different forms for the reward (SI). The approximate solution is used to demonstrate that the stinging response increases with starvation under broad conditions, i.e. as long as $r(s)$ and $p(a)$ are concave functions and c(a) is convex (see ***Supplementary Information***). To exemplify the importance of acting optimally to save resources, we considered two agents, one acting optimally and one acting randomly i.e. shooting with a number of nematocysts uniformly distributed between a_{min} and a_{max}. Both agents start at the same starvation state ($s = 0.9$ in **Figure 2D**) and use on average the same number of nematocysts, but the random agent reaches starvation typically in tens of steps, whereas the optimal agent converges to a steady state (around $s = 0.3$ in the figure) and hardly ever reaches severe starvation.

To model *Exaiptasia*, we assume the agent stings for defense, thus the associated Markov process models transitions between the states of safety, which we indicate with *L,* and danger, which we indicate with *D*. The state of starvation is not affected by stinging and instead is dictated by a separate process that relies on symbionts and which we do not model. Similar to the previous model, the agent chooses an action, a, representing the intensity of the attack. Each attack has a likelihood to succeed $p(a)$ and an associated cost $c(a) = c_0 a$ where c_0 is the cost of full discharge of all nematocysts at once. A successful attack allows the animal to remain in state L and receive a unit reward; a failed attack leads to state D and penalty -1. F is an absorbing state hence $V^*(F) = 0$. The optimal value and action in state L follow:

$$V^*(L) = \max_a(p(a)(-c_0 a + \gamma V^*(L) + 1) + (1 - p(a))(-1 - c_0 a)) \tag{2}$$

$$a^*(L) = \operatorname*{argmax}_a(p(a)(-c_0 a + \gamma V^*(L) + 1) + (1 - p(a))(-1 - c_0 a))$$

Zeroing the derivative of the argument on the r.h.s. of equation (2) leads to

$$-c_0 + p'(a^*)(\gamma V^*(L) + 2) = 0$$

$$V^*(L) = -c_0 a^* + p(a^*)(\gamma V^*(L) + 1) + (1 - p(a^*))$$

Here, $p(a)$ is the probability of success of action a, hence it goes from $p(0) = 0$ to $p(1) = p_M < 1$. Assuming a specific form $p = p_M a(2 - a)$ leads to the specific solution $a^* = K - \sqrt{K^2 - A}$ where $K = \frac{2-\gamma}{c_0 \gamma}$ and $A = -\frac{1}{\gamma p_M} + 2K$. If c_0 is constant, there is a non-trivial optimal action as long as $c_0 < 2p_M(2 - \gamma)$ and clearly the optimal action does not depend on starvation (constant solution in Figure 2E, right, with $c_0 = 1$; $\gamma = 0.99$ and $p_M = 0.8$).

Stinging predators does not improve nutritional state, thus transitions among different starvation states are not modelled for defensive stinging, but instead rely heavily on symbionts. However, to capture subtle effects of starvation on defensive stinging, we note that the cost of discharging nematocysts may still depend parametrically on whatever state of starvation the agent happens to be in. In this case, $c_0 = c_0(s)$ and under the assumption that the cost increases with starvation, we find that optimal defensive stinging always decrease with starvation, for any functional form of p (see ***Supplementary Information*** for more details). We applied the same cost to predatory stinging and found that it still increases for moderate increase of $c_0(s)$ with s. The result is exemplified in **Figure 2C** using a functional form for $c_0(s)$ that is obtained by fitting the experimental data as described in the ***Supplementary Information***. Hence for defensive stinging, the optimal strategy is either independent of starvation or may decrease with starvation.

We then considered more intense increase of $c_0(s)$ with s for both models. In contrast to defensive stinging, we find that predatory stinging increases with starvation for mild increase $c_0(s)$ and decreases with starvation if the cost increase is too steep (see ***Supplementary Information*** discussion and Supplementary Figure 3 for a comparison with 4 different cost functions).

Statistical analysis

Data were analyzed with Clampfit (Axon Instruments), Prism (GraphPad), or QuantaSoft (BioRad Laboratories) and are represented as mean ± sem. *n* represents independent experiments for the number of cells/patches or behavioral trials. Data were considered significant if $p < 0.05$ using paired or unpaired two-tailed Student's t-tests or one- or two-way ANOVAs. All significance tests were justified considering the experimental design and we assumed normal distribution and variance, as is common for similar

experiments. Sample sizes were chosen based on the number of independent experiments required for statistical significance and technical feasibility.

Data availability

Deep sequencing data are available via the Sequence Read Archive (SRA) repository under the BioProject accession code PRJNA945904. All plasmids are available upon request. Further requests for resources and reagents should be directed to and will be fulfilled by the corresponding author, NWB (nbellono@harvard.edu). The Matlab code to obtain the optimal predicted stinging according to our Markov Decision Process is available from https://zenodo.org/record/8177567.

Acknowledgments: We thank B. Walsh and P. Kilian for assistance with animal husbandry, A. Whipple and D. Loftus with guidance for ddPCR experiments, A. Grearson for illustrations and photographs, K. Koenig and M. Martindale, and the Marine Biological Laboratory for providing animals. We also thank the Harvard Center for Biological Imaging (RRID:SCR_018673), Histology Core at the Harvard Department of Stem Cell and Regenerative Biology, and The Bauer Core Facility at Harvard University for infrastructure and experimental support. This research was supported by grants to NWB from the New York Stem Cell Foundation, Searle Scholars Program, and the NIH (R35GM142697), fellowships to LH from NSF Graduate Research Fellowship Program and Physics of Living Systems (PoLS) Graduate Fellowship and the Simmons Award at the Harvard Center for Biological Imaging, grants to AS from the European Research Council (ERC) under the European Union's Horizon 2020 research and innovation programme (grant agreement No 101002724 RIDING), the Air Force Office of Scientific Research under award number FA8655-20-1-7028, and the National Institutes of Health (NIH) under award number R01DC018789.

Author Contributions: LH, CA, SK, KW, and NWB contributed to physiological studies. LH contributed to behavioral, histological, and molecular studies. LH and WV contributed to phylogenetic, transcriptomic, and genomic studies. YQ and AS contributed to mathematical modelling studies. All authors were involved with writing or reviewing the manuscript.

Competing Interests: The authors declare no competing financial interests.

References

Aguilar-Camacho JM, Foreman K, Jaimes-Becerra A, Aharoni R, Gründer S, Moran Y (2023) Functional analysis in a model sea anemone reveals phylogenetic complexity and a role in cnidocyte discharge of DEG/ENaC ion channels. Commun Biol 6:17.

Babonis LS, Enjolras C, Ryan JF, Martindale MQ (2022) A novel regulatory gene promotes novel cell fate by suppressing ancestral fate in the sea anemone *Nematostella vectensis*. Proc Natl Acad Sci 119:e2113701119.

Babonis LS, Martindale MQ (2014) Old Cell, New Trick? Cnidocytes as a Model for the Evolution of Novelty. Integr Comp Biol 54:714–722.

Baumgarten S, Simakov O, Esherick LY, Liew YJ, Lehnert EM, Michell CT, Li Y, Hambleton EA, Guse A, Oates ME, Gough J, Weis VM, Aranda M, Pringle JR, Voolstra CR (2015) The genome of *Aiptasia*, a sea anemone model for coral symbiosis. Proc Natl Acad Sci 112:11893–11898.

Beckmann A, Özbek S (2012) The Nematocyst: a molecular map of the Cnidarian stinging organelle. Int J Dev Biol 56:577–582.

Bedgood SA, Bracken MES, Ryan WH, Levell ST, Wulff J (2020) Nutritional drivers of adult locomotion and asexual reproduction in a symbiont-hosting sea anemone Exaiptasia diaphana. Mar Biol 167:39.

Bellman R (2003) Dynamic Programming. Dover.

Botton-Amiot G, Martinez P, Sprecher SG (2023) Associative learning in the cnidarian *Nematostella vectensis*. Proc Natl Acad Sci 120:e2220685120.

Bouchard C, Price RB, Moneypenny CG, Thompson LF, Zillhardt M, Stalheim L, Anderson PAV (2006) Cloning and functional expression of voltage-gated ion channel subunits from cnidocytes of the Portuguese Man O'War Physalia physalis. J Exp Biol 209:2979–2989.

Bray NL, Pimentel H, Melsted P, Pachter L (2016) Near-optimal probabilistic RNA-seq quantification. Nat Biotechnol 34:525–527.

Bucher M, Wolfowicz I, Voss PA, Hambleton EA, Guse A (2016) Development and Symbiosis Establishment in the Cnidarian Endosymbiosis Model Aiptasia sp. Sci Rep 6:19867.

Buchfink B, Xie C, Huson DH (2015) Fast and sensitive protein alignment using DIAMOND. Nat Methods 12:59–60.

Buraei Z, Yang J (2010) The β Subunit of Voltage-Gated Ca2+ Channels. Physiol Rev 90:1461–1506.

Cartwright P, Halgedahl SL, Hendricks JR, Jarrard RD, Marques AC, Collins AG, Lieberman BS (2007) Exceptionally Preserved Jellyfishes from the Middle Cambrian Humphries S, ed. PLoS ONE 2:e1121.

Columbus-Shenkar YY, Sachkova MY, Macrander J, Fridrich A, Modepalli V, Reitzel AM, Sunagar K, Moran Y (2018) Dynamics of venom composition across a complex life cycle. eLife 7:e35014.

Damian-Serrano A, Hetherington ED, Choy CA, Haddock SHD, Lapides A, Dunn CW (2022) Characterizing the secret diets of siphonophores (Cnidaria: Hydrozoa) using DNA metabarcoding Dam HG, ed. PLOS ONE 17:e0267761.

Darling JA, Reitzel AR, Burton PM, Mazza ME, Ryan JF, Sullivan JC, Finnerty JR (2005) Rising starlet: the starlet sea anemone, Nematostella vectensis. BioEssays 27:211–221.

Ebert AM, McAnelly CA, Srinivasan A, Mueller RL, Garrity DB, Garrity DM (2008) The calcium channel β2 (CACNB2) subunit repertoire in teleosts. BMC Mol Biol 9:38.

Foell JD, Balijepalli RC, Delisle BP, Yunker AMR, Robia SL, Walker JW, McEnery MW, January CT, Kamp TJ (2004) Molecular heterogeneity of calcium channel β-subunits in canine and human heart: evidence for differential subcellular localization. Physiol Genomics 17:183–200.

Fraune S, Forêt S, Reitzel AM (2016) Using Nematostella vectensis to Study the Interactions between Genome, Epigenome, and Bacteria in a Changing Environment. Front Mar Sci 3.

Giebel GEM, Thorington GU, Lim RY, Hessinger DA (1988) Control of Cnida Discharge: II. Microbasic p-Mastigophore Nematocysts are Regulated by Two Classes of Chemoreceptors. Biol Bull 175:132–136.

Gitter AH, Oliver D, Thurm U (1994) Calcium- and voltage-dependence of nematocyst discharge in Hydra vulgaris. J Comp Physiol A 175.

Grabherr MG et al. (2011) Full-length transcriptome assembly from RNA-Seq data without a reference genome. Nat Biotechnol 29:644–652.

Grajales A, Rodríguez E (2014) Morphological revision of the genus Aiptasia and the family Aiptasiidae (Cnidaria, Actiniaria, Metridioidea). Zootaxa 3826:55.

Helton TD, Horne WA (2002) Alternative Splicing of the β_4 Subunit Has α_1 Subunit Subtype-Specific Effects on Ca^{2+} Channel Gating. J Neurosci 22:1573–1582.

Helton TD, Kojetin DJ, Cavanagh J, Horne WA (2002) Alternative Splicing of a b4 Subunit Proline-Rich Motif Regulates Voltage-Dependent Ca2+ Channels Gating and Toxin Block of Cav2. J Neurosci 22:9331–9339.

Hoang DT, Chernomor O, von Haeseler A, Minh BQ, Vinh LS (2018) UFBoot2: Improving the Ultrafast Bootstrap Approximation. Mol Biol Evol 35:518–522.

694 Holstein T, Tardent P (1984) An Ultrahigh-Speed Analysis of Exocytosis: Nematocyst Discharge. Science 223:830–
695 833.
696 Jékely G, Keijzer F, Godfrey-Smith P (2015) An option space for early neural evolution. Philos Trans R Soc B Biol
697 Sci 370:20150181.
698 Jeziorski MC, Greenberg RM, Clark KS, Anderson PAV (1998) Cloning and Functional Expression of a Voltage-
699 gated Calcium Channel α1 Subunit from Jellyfish. J Biol Chem 273:22792–22799.
700 Kalyaanamoorthy S, Minh BQ, Wong TKF, von Haeseler A, Jermiin LS (2017) ModelFinder: fast model selection for
701 accurate phylogenetic estimates. Nat Methods 14:587–589.
702 Kass-Simon G, Scappaticci AA (2002) The behavioral and developmental physiology of nematocysts. 80:23.
703 Katoh K, Standley DM (2013) MAFFT Multiple Sequence Alignment Software Version 7: Improvements in
704 Performance and Usability. Mol Biol Evol 30:772–780.
705 Lam J, Cheng Y-W, Chen W-NU, Li H-H, Chen C-S, Peng S-E (2017) A detailed observation of the ejection and
706 retraction of defense tissue acontia in sea anemone (*Exaiptasia pallida*). PeerJ 5:e2996.
707 Langmead B, Salzberg SL (2012) Fast gapped-read alignment with Bowtie 2. Nat Methods 9:357–359.
708 Leclère L et al. (2019) The genome of the jellyfish Clytia hemisphaerica and the evolution of the cnidarian life-cycle.
709 Nat Ecol Evol 3:801–810.
710 Lehnert EM, Burriesci MS, Pringle JR (2012) Developing the anemone Aiptasia as a tractable model for cnidarian-
711 dinoflagellate symbiosis: the transcriptome of aposymbiotic A. pallida. BMC Genomics 13:271.
712 Lubbock R, Amos WB (1981) Removal of bound calcium from nematocyst contents causes discharge. Nature
713 290:500–501.
714 Lubbock R, Gupta BL, Hall TA (1981) Novel role of calcium in exocytosis: mechanism of nematocyst discharge as
715 shown by x-ray microanalysis. Proc Natl Acad Sci 78:3624–3628.
716 Madeira F, Pearce M, Tivey ARN, Basutkar P, Lee J, Edbali O, Madhusoodanan N, Kolesnikov A, Lopez R (2022)
717 Search and sequence analysis tools services from EMBL-EBI in 2022. Nucleic Acids Res 50:W276–W279.
718 Matthews JL, Sproles AE, Oakley CA, Grossman AR, Weis VM, Davy SK (2016) Menthol-induced bleaching rapidly
719 and effectively provides experimental aposymbiotic sea anemones (*Aiptasia* sp.) for symbiosis
720 investigations. J Exp Biol 219:306–310.
721 Minh BQ, Schmidt HA, Chernomor O, Schrempf D, Woodhams MD, von Haeseler A, Lanfear R (2020) IQ-TREE 2:
722 New Models and Efficient Methods for Phylogenetic Inference in the Genomic Era Teeling E, ed. Mol Biol
723 Evol 37:1530–1534.
724 Muscatine L, R. McCloskey L, E. Marian R (1981) Estimating the daily contribution of carbon from zooxanthellae to
725 coral animal respiration1: Muscatine et al. Limnol Oceanogr 26:601–611.
726 Nüchter T, Benoit M, Engel U, Özbek S, Holstein TW (2006) Nanosecond-scale kinetics of nematocyst discharge.
727 Curr Biol 16:R316–R318.
728 Östman C (2000) A guideline to nematocyst nomenclature and classification, and some notes on the systematic
729 value of nematocysts. Sci Mar 64:31–46.
730 Ozment E, Tamvacakis AN, Zhou J, Rosiles-Loeza PY, Escobar-Hernandez EE, Fernandez-Valverde SL,
731 Nakanishi N (2021) Cnidarian hair cell development illuminates an ancient role for the class IV POU
732 transcription factor in defining mechanoreceptor identity. eLife 10:e74336.
733 Pallasdies F, Goedeke S, Braun W, Memmesheimer R-M (2019) From single neurons to behavior in the jellyfish
734 Aurelia aurita. eLife 8:e50084.
735 Pantin CFA (1942) Excitation of Nematocysts. Nature 3769:109.
736 Plachetzki DC, Fong CR, Oakley TH (2012) Cnidocyte discharge is regulated by light and opsin-mediated
737 phototransduction. BMC Biol 10:17.
738 Sandberg DM, Kanciruk P, Mariscal RN (1971) Inhibition of Nematocyst Discharge correlated with Feeding in a Sea
739 Anemone, Calliactis tricolor (Leseur). Nature 232:263–265.
740 Schindelin J, Arganda-Carreras I, Frise E, Kaynig V, Longair M, Pietzsch T, Preibisch S, Rueden C, Saalfeld S,
741 Schmid B, Tinevez J-Y, White DJ, Hartenstein V, Eliceiri K, Tomancak P, Cardona A (2012) Fiji: an open-
742 source platform for biological-image analysis. Nat Methods 9:676–682.
743 Schüler A, Schmitz G, Reft A, Özbek S, Thurm U, Bornberg-Bauer E (2015) The Rise and Fall of TRP-N, an
744 Ancient Family of Mechanogated Ion Channels, in Metazoa. Genome Biol Evol 7:1713–1727.
745 Shick JM, Dykens JA (1984) Photobiology of the Symbiotic Sea Anemone Anthopleura elegantissima:
746 Photosynthesis, Respiration, and Behavior under Intertidal Conditions. Biol Bull 166:608–619.
747 Siller A, Hofer NT, Tomagra G, Burkert N, Hess S, Benkert J, Gaifullina A, Spaich D, Duda J, Poetschke C, Vilusic
748 K, Fritz EM, Schneider T, Kloppenburg P, Liss B, Carabelli V, Carbone E, Ortner NJ, Striessnig J (2022)
749 β2-subunit alternative splicing stabilizes Cav2.3 Ca2+ channel activity during continuous midbrain
750 dopamine neuron-like activity. eLife 11:e67464.
751 Song L, Florea L (2015) Rcorrector: efficient and accurate error correction for Illumina RNA-seq reads.
752 GigaScience 4:48.

753 Steele RE, David CN, Technau U (2011) A genomic view of 500 million years of cnidarian evolution. Trends Genet
754 27:7–13.
755 Steen G (1988) The Bioenergetics of Symbiotic Sea Anemones (Anthozoa: Actiniaria). Symbiosis 5:103–142.
756 Stefanik DJ, Wolenski FS, Friedman LE, Gilmore TD, Finnerty JR (2013) Isolation of DNA, RNA and protein from
757 the starlet sea anemone Nematostella vectensis. Nat Protoc 8:892–899.
758 Sutton, Barto AG (2018) Reinforcement learning: An introduction. MIT Press.
759 Takahashi SX, Mittman S, Colecraft HM (2003) Distinctive Modulatory Effects of Five Human Auxiliary β2 Subunit
760 Splice Variants on L-Type Calcium Channel Gating. Biophys J 84:3007–3021.
761 Tardent P (1995) The cnidarian cnidocyte, a hightech cellular weaponry. BioEssays 17:351–362.
762 Technau U, Steele RE (2012) Evolutionary crossroads in developmental biology: Cnidaria. Development 139:4491–
763 4491.
764 Thorington GU, Hessinger DA (1988) Control of Cnida Discharge: I. Evidence for Two Classes of Chemoreceptor.
765 Biol Bull 174:163–171.
766 Vendel AC, Terry MD, Striegel AR, Iverson NM, Leuranguer V, Rithner CD, Lyons BA, Pickard GE, Tobet SA,
767 Horne WA (2006) Alternative Splicing of the Voltage-Gated Ca^{2+} Channel β_4 Subunit Creates a Uniquely
768 Folded N-Terminal Protein Binding Domain with Cell-Specific Expression in the Cerebellar Cortex. J
769 Neurosci 26:2635–2644.
770 Wang H, Swore J, Sharma S, Szymanski JR, Yuste R, Daniel TL, Regnier M, Bosma MM, Fairhall AL (2023) A
771 complete biomechanical model of *Hydra* contractile behaviors, from neural drive to muscle to movement.
772 Proc Natl Acad Sci 120:e2210439120.
773 Watson GM, Hessinger DA (1989) Cnidocyte Mechanoreceptors are Tuned to the Movements of Swimming Prey
774 by Chemoreceptors. Science 243:1589–1591.
775 Watson GM, Hessinger DA (1994) Evidence for calcium channels involved in regulating nematocyst discharge.
776 Comp Biochem Physiol A Physiol 107:473–481.
777 Watson GM, Mire-Thibodeaux P (1994) The Cell Biology of Nematocysts. In: International Review of Cytology, pp
778 275–300. Elsevier.
779 Weber J (1990) Poly(gamma-glutamic acid)s are the major constituents of nematocysts in Hydra (Hydrozoa,
780 Cnidaria). J Biol Chem 265:9664–9669.
781 Weir K, Dupre C, van Giesen L, Lee AS-Y, Bellono NW (2020) A molecular filter for the cnidarian stinging
782 response. eLife 9:e57578.
783 Westfall JA (2004) Neural pathways and innervation of cnidocytes in tentacles of sea anemones. Hydrobiologia
784 530:5.
785 Westfall JA, Elliott CF, Carlin RW (2002) Ultrastructural evidence for two-cell and three-cell neural pathways in the
786 tentacle epidermis of the sea anemone Aiptasia pallida. J Morphol 251:83–92.
787 Westfall JA, Landers DD, McCallum JD (1998) Different nematocytes have different synapses in the sea anemone
788 Aiptasia pallida (Cnidaria, Anthozoa). J Morphol 238:53–62.
789 Wu TD, Watanabe CK (2005) GMAP: a genomic mapping and alignment program for mRNA and EST sequences.
790 Bioinformatics 21:1859–1875.
791

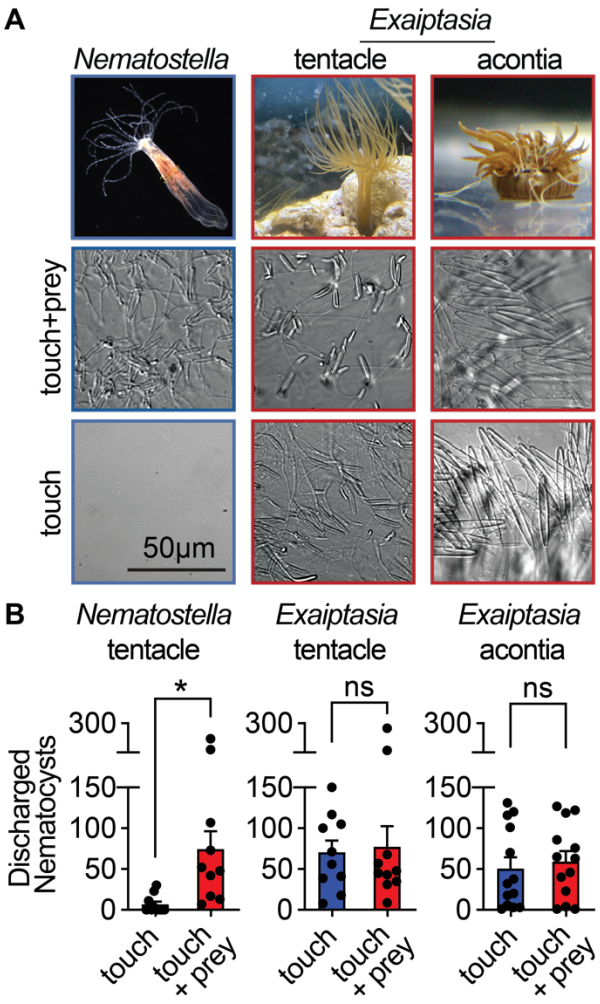

Figure 1. Comparative sea anemone stinging behavior.

A) *Nematostella vectensis* stings with tentacles while *Exaiptasia diaphana* also stings with acontia filaments that are ejected from its body for defense. *Left*: *Nematostella* nematocyte discharge was only observed in response to simultaneous prey chemicals and touch stimuli. *Middle, Right*: *Exaiptasia* nematocyte discharge from tentacles and acontia occurred irrespective of prey cues (touch alone). Scale bar = 50µm.

B) *Nematostella* nematocyte discharge was elicited by simultaneous touch and prey chemical stimuli (n = 10 trials). *Exaiptasia* tentacle (n = 10) and acontia (n = 13) nematocytes discharged only to touch, with or without prey chemicals. $p < 0.05$ for *Nematostella*, paired two-tailed student's t-test. Data represented as mean ± sem.

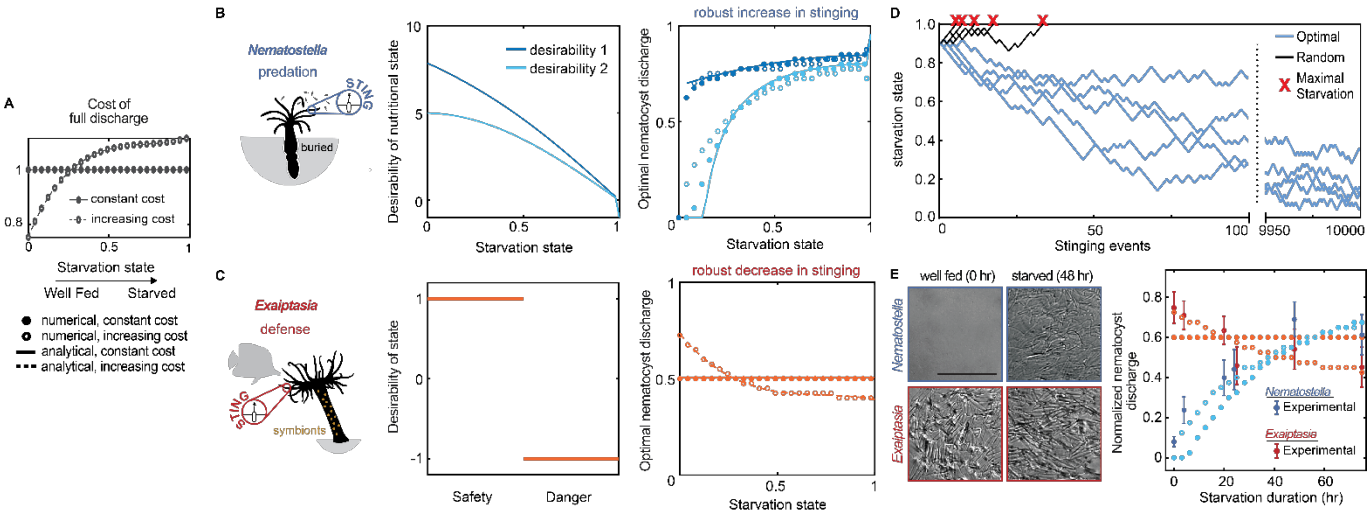

Figure 2. *Nematostella* stinging is regulated by predation while *Exaiptasia* stings for defense.

A) The cost of stinging is $c = c_o a$, where c_o is the cost for full nematocyte discharge and it either does not change (solid lines filled circles) or increases slightly (dashed lines empty circles) with starvation state. These symbols are used throughout the figure to represent each cost function. The increasing cost is obtained by fitting the Exaiptasia behavior (*see fitting procedure in* ***Supplementary Information***).

B) *Left: Nematostella* burrows in the substrate and stings for predation. *Center*: Desirability of nutritional state, or reward, decreases with starvation. Two examples are shown: example 1, $r(s) = 10\, tan^{-1}\,(1-s)$; example 2, $r(s) = 5\, cos\left(\frac{s\pi}{2}\right)$. *Right*: Predicted optimal stinging obtained by solving equation (1) with numerical simulations (circles) and approximate analytical solutions (lines) assuming: $p(a) = p_M\, a(2-a)$ and $p_M = 0.8$; $c = c_0 a$ with cost for full discharge c_0 matching panel A (full circles and solid lines for constant cost; empty circles for increasing cost); reward in Left panels (colors match). For all reward and cost functions, optimal predatory stinging increases with starvation under broad assumptions (*see* ***Supplementary Information***).

C) *Left: Exaiptasia diaphana* relies heavily on endosymbiotic algae for nutrients and stings primarily for defense. *Center:* We assumed there are two states, safety (L), and danger (D). The state of safety can transition to danger, but not the other way around. We assumed the agent obtains reward 1 in state L and penalty -1 in state D. *Right:* Predicted optimal stinging obtained by solving equation (2) with numerical simulations (circles) and analytical solutions (lines). Styles match the costs in panel A; we assume $p(a) = p_M\, a(2-a)$ and $p_M = 0.8$ as before. Optimal defensive stinging is constant or decreases with starvation under broad assumptions (*see* ***Supplementary Information***).

D) Examples of optimal (blue) versus random (black) predatory stinging. Each agent (anemone) starts with $s = 0.9$, and stings sequentially for many events (represented on the *x* axis). The random agent almost always reaches maximal starvation before time 50 events (grey lines, five examples shown). In comparison, the optimal agent effectively never starves due to a successful stinging strategy optimized for predation (blue lines, five examples shown, parameters as in panel B, curve with matching color).

E) *Left: Nematostella* nematocyte discharge was affected by prey availability while *Exaiptasia* stung at a similar rate regardless of feeding. $p < 0.0001$ for *Nematostella*, two-way ANOVA with post hoc Bonferroni test (n = 10 animals, data represented as mean ± sem). *Right*: Experimental data (circles with error bars representing standard deviation) are well fit by normalized optimal

nematocyst discharge predicted from MDP models for both *Exaiptasia* (orange full and empty circles for constant and increasing cost, panel A) and *Nematostella* (light blue full and empty circles for constant and increasing cost, panel A and reward 2 in panel B). We match the last experimental data point to $s = 0.5$, the precise value of this parameter is irrelevant as long as it is smaller than 1, representing that animals are not severely starved during the experiment.

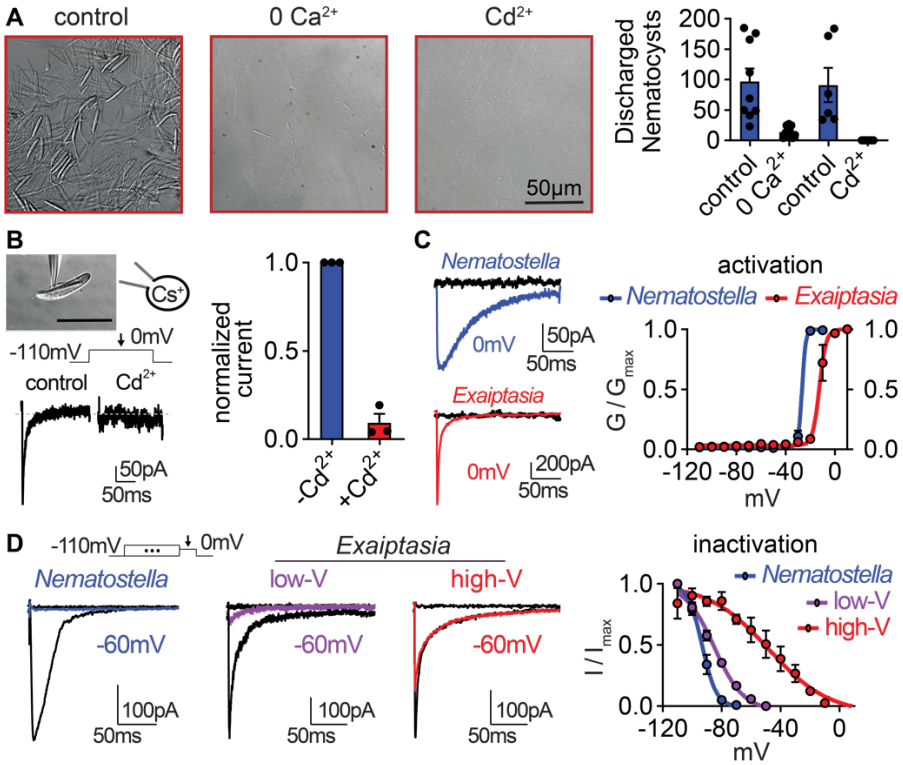

Figure 3. *Exaiptasia* nematocyte voltage-gated Ca^{2+} currents exhibit minimal steady-state inactivation compared with *Nematostella*.

A) Touch-elicited *Exaiptasia* tentacle nematocyte discharge was blocked in the absence of Ca^{2+} ($p < 0.01$, paired two-tailed student's t-test, n = 9) or by addition of the Ca_V channel blocker Cd^{2+} (500µM, $p < 0.05$, paired two-tailed student's t-test, n = 6). Scale bar = 50µm.

B) *Top:* Representative patch clamp experiment from an *Exaiptasia* nematocyte. Scale bar = 20µm. *Bottom*: Nematocyte voltage-gated currents elicited by a maximally activating 0mV pulse were blocked by Cd^{2+} (n = 3, $p < 0.01$, paired two-tailed student's t-test).

C) Nematocyte voltage-gated currents elicited by -120mV (black) or 0mV pulses (colored). Conductance-voltage curves for *Nematostella* nematocyte ($V_{a1/2}$ = -26.54 ± 0.78mV, n = 3) and *Exaiptasia* nematocyte ($V_{a1/2}$ = -12.47 ± 0.70mV, n = 3).

D) Nematocyte voltage-gated currents elicited by a maximally activating voltage pulse following 1 s pre-pulses to −110 mV (max current, black), −50 mV (colored), or 20 mV (inactivated, no current). *Nematostella* nematocytes inactivated at very negative voltages ($V_{i1/2}$ = -93.22 ± 0.42mV, n = 7) while *Exaiptasia* contained two populations of nematocytes: low-voltage threshold ($V_{i1/2}$ = -84.94 ± 0.70mV, n = 4), and high-voltage threshold ($V_{i1/2}$ = -48.17 ± 3.32mV, n = 3). Data represented as mean ± sem.

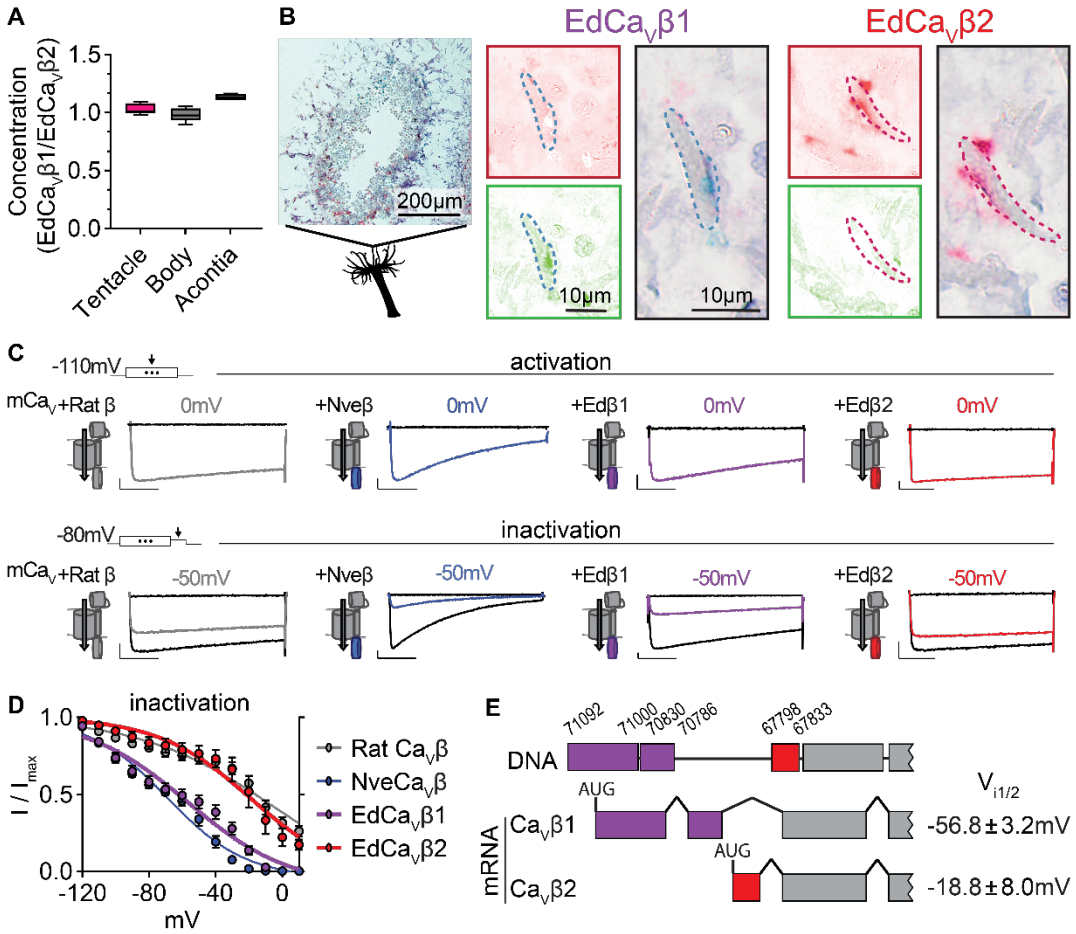

Figure 4. *Exaiptasia* expresses a Ca_V β subunit splice isoform that confers weak voltage-dependent inactivation.

A) ddPCR ratio of concentrations of Ca_V β subunit 1 and 2 mRNAs was similar in tentacle (n = 5), body (n = 5), and acontia (n = 4 animals) tissue samples.

B) $EdCa_V\beta1$ and $EdCa_V\beta2$ localized to distinct nematocytes in *Exaiptasia* tentacle cross section, as visualized by BaseScope *in situ* hybridization. Representative nematocyte expressing $EdCa_V\beta1$ (green) or $EdCa_V\beta2$ (red). Representative of 3 animals.

C) Voltage-gated currents from heterologously-expressed chimeric mammalian Ca_V (mCa_V) with different β subunits: rat (*Rattus norvegicus*), *Nematostella* (Nve), *Exaiptasia* $EdCa_V\beta1$ or $EdCa_V\beta2$. *Top*: Currents elicited by voltage pulses to -120mV (no current, black) and maximally activating 0mV (colored). *Bottom*: Voltage-gated currents elicited by a maximally activating voltage pulse following 1 s pre-pulses to −110 mV (max current, black), −50 mV (colored), or 20 mV (inactivated, no current, black). Scale bars = 100pA, 50ms.

D) *Exaiptasia* Ca_V β subunit splice isoforms confer distinct inactivation: *Nematostella* β subunit ($V_{i1/2}$ = -68.93 ± 1.53mV, n = 5) and Rat β2a subunit ($V_{i1/2}$ = -2.98 ± 13.51mV, n = 12) and $EdCa_V\beta1$ ($V_{i1/2}$ = -56.76 ± 3.18mV, n = 8), and $EdCa_V\beta2$ ($V_{i1/2}$ = -18.84 ± 8.00mV, n = 5). Data represented as mean ± sem.

E) Genomic alignment of *Exaiptasia* β subunit isoforms showed that alternative splicing of the N-terminus region was associated with distinct inactivation: $Ca_V\beta1$ (long N-term) had low-voltage steady-state inactivation similar to *Nematostella*, while $Ca_V\beta2$ (short N-term) exhibited more depolarized steady-state inactivation, matching its mammalian orthologue. Genomic loci listed above sequence.

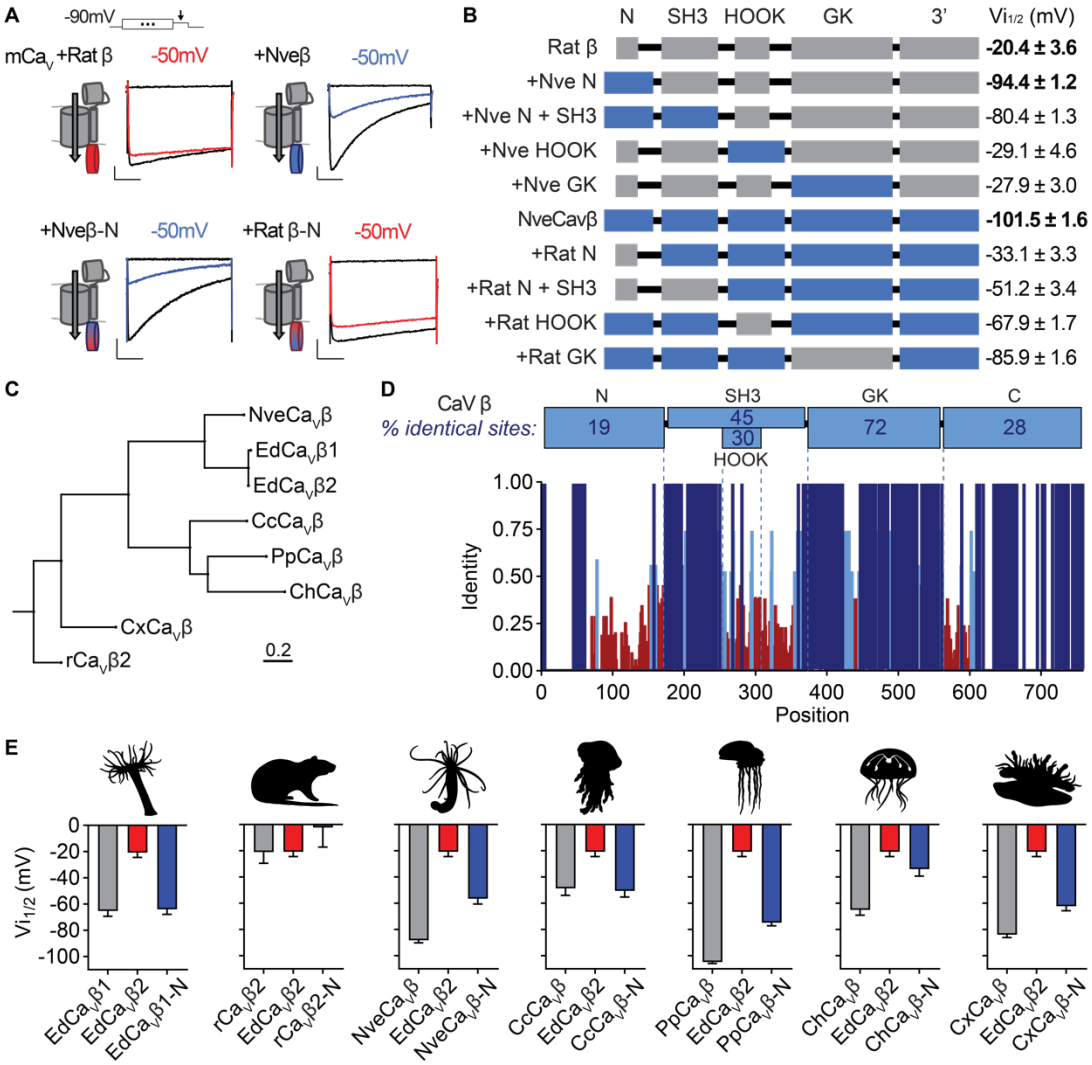

Figure 5. Cnidarian Ca_V β subunit N-termini confer unique inactivation properties.

A) Voltage-gated currents from heterologously expressed Ca_V channels with *Nematostella*-rat chimeric β subunits demonstrate that the *Nematostella* N-terminus is sufficient to drive inactivation at negative voltages. Currents shown in response to 10 mV voltage pulses following 1 s pre-pulses to −130 mV (max current, black), −50 mV (colored), or 0 mV (inactivated, no current, black). Scale bars = 100pA, 50ms.

B) Diagram of Ca_V *Nematostella*-rat β subunit domain swaps and resulting $V_{i1/2}$ values. The *Nematostella* β subunit N-terminus is required and sufficient for uniquely hyperpolarized Ca_V inactivation properties ($p < 0.001$ for average $V_{i1/2}$ values across mutant beta subunits, one-way ANOVA with post-hoc Tukey test, n = 2-8 cells).

C) Phylogenetic tree of β subunit sequences obtained from several species of cnidarians. Abbreviations of species: Nve, *Nematostella vectensis*; Ed, *Exaiptasia diaphana*; Cc, *Cyanea capillata* (jellyfish); Pp, *Physalia physalis* (siphonophore); Ch, *Clytia hemisphaerica* (jellyfish); Cx, *Cassiopea xamachana* (jellyfish); r, *Rattus norvegicus*.

D) *Top*: Percentage of identity between amino acid sequences across β subunit protein domains for $NveCa_V\beta$, $EdCa_V\beta1$, $EdCa_V\beta2$, $CcCa_V\beta$, $PpCa_V\beta$, $ChCa_V\beta$, $CxCa_V\beta2$, $rCa_V\beta2$. *Bottom*: Fraction of identity of amino acids across sites of the β subunit protein.

E) Cnidarian Ca_V β N-termini shift depolarized, weak voltage-dependent inactivation of Ca_V channels containing $EdCa_V\beta2$ to more negative voltages. Voltage-dependent inactivation ($V_{i1/2}$) of

909 heterologously-expressed Ca_Vs with WT $EdCa_V\beta2$, β subunits from the indicated cnidarians, and
910 chimeras with their N-termini on $EdCa_V\beta2$ ($p < 0.0001$ for average $V_{i1/2}$ values with multiple
911 comparisons against WT $EdCa_V\beta2$ mean, one-way ANOVA with Bartlett's test and post-hoc
912 Tukey test, n = 4-9 cells). Data represented as mean ± sem.

Supplementary Information Text: Markov Decision Processes modeling defensive vs predatory stinging.

915

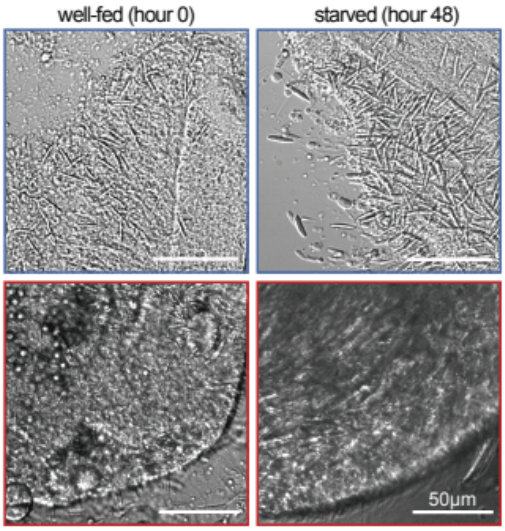

916

917 **Figure 2S1. Modulation of *Nematostella* and *Exaiptasia* stinging is not due to changes in the**
918 **abundance of nematocytes.**

919 Nematocytes were highly abundant in tentacles from *Nematostella (top)* and *Exaiptasia (bottom)* before
920 and after starvation. Representative of n = 3 animals. Scale bar = 50µm.

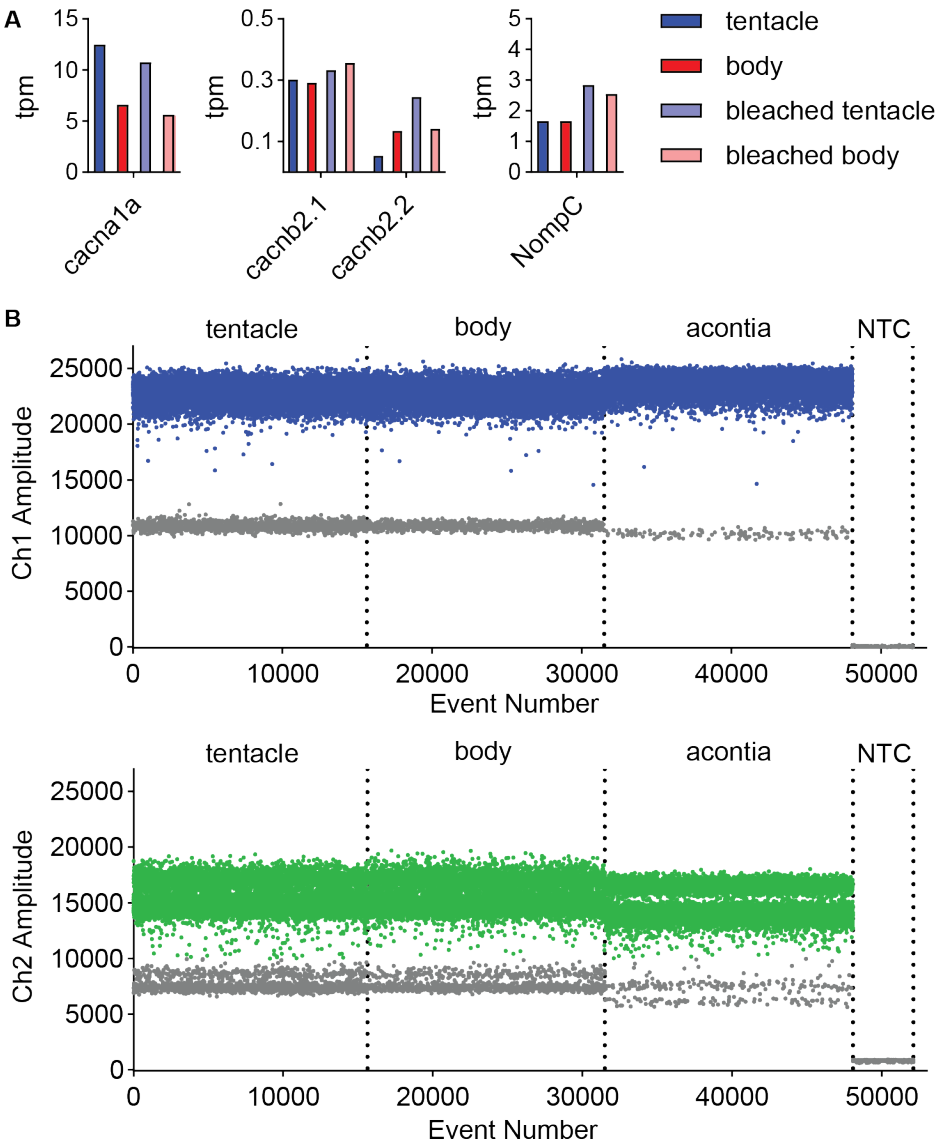

Figure 4S1. Transcriptomic and molecular analyses of *Exaiptasia* β subunit isoforms.

A) mRNA expression (transcripts per million, TPM) of voltage-gated calcium (Ca_V) channel α and β subunits in *Exaiptasia* tentacle (nematocyte abundant, blue), body (nematocyte non-abundant, red), bleached (minimal symbionts) tentacle (light blue), bleached body (light red) tissues. The Ca_V α subunit was identified by homology to the sequence of the cnidarian $Ca_V2.1$ homolog found enriched in *Nematostella* nematocyte-rich tissues (Weir et al., 2020). NompC, the putative mechanoreceptor in *Nematostella* nematocytes (Schüler et al., 2015; Weir et al., 2020), was also detected in *Exaiptasia* tentacles.

B) Representative plots of fluorescent amplitude across event number (droplet events) from amplification of unique regions of $EdCa_V\beta1$ (Ch1, *Top*) and $EdCa_V\beta2$ (Ch2, *Bottom*) sequences using droplet digital PCR (ddPCR, Bio-Rad Laboratories). Individual lanes correspond to tentacle RNA, body RNA, acontia RNA, and no template control (NTC). Blue and green points indicate positive PCR droplets after thresholding and gray points indicate negative droplets.

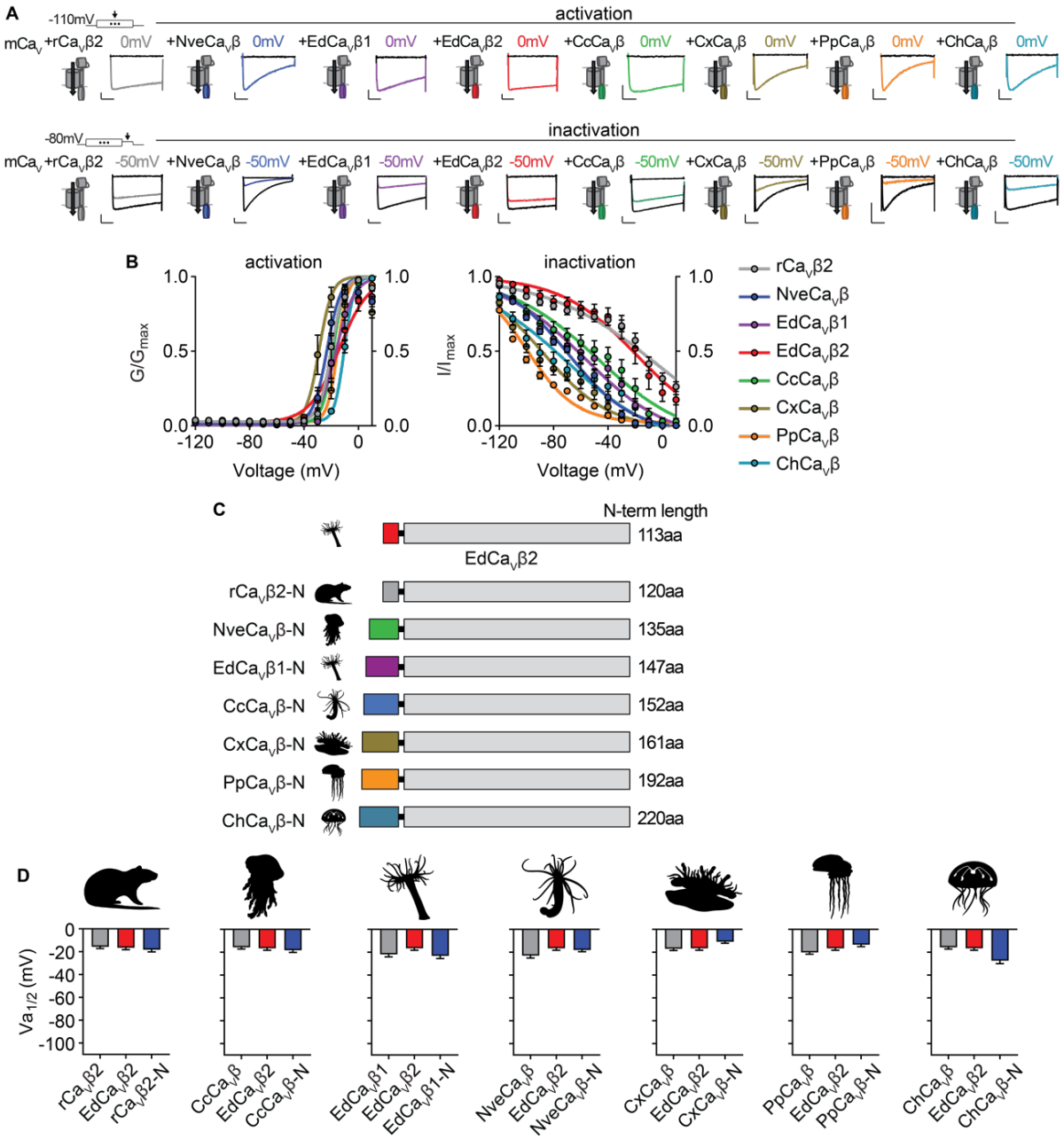

Figure 5S1. Voltage-dependent activation of Ca_V channels is conserved across cnidarian β subunits.

A) *Top*: Voltage-gated currents from heterologously-expressed chimeric Ca_Vs with the indicated β subunits elicited by voltage pulses to -120mV (no current, black) and 0mV (colored). Abbreviations of species: Nve, *Nematostella vectensis*; Ed, *Exaiptasia diaphana*; Cc, *Cyanea capillata* (jellyfish); Pp, *Physalia physalis* (siphonophore); Ch, *Clytia hemisphaerica* (jellyfish); Cx, *Cassiopea xamachana* (jellyfish); r, *Rattus norvegicus*. *Bottom*: Voltage-gated currents elicited by a maximally activating voltage pulse following 1 s pre-pulses to −110 mV (max current, black), −50 mV (colored), or 20 mV (inactivated, no current, black). Scalebars = 100pA, 50ms.

B) Activation and inactivation curves for heterologously-expressed chimeric Ca_Vs with different β subunits. Activation: $rCa_V\beta2$ $V_{a1/2}$ = -19.76 ± 1.16mV, n = 12; $NveCa_V\beta$ $V_{a1/2}$ = -23.07 ± 1.16mV, n = 5; $EdCa_V\beta1$ $V_{a1/2}$ = -18.27 ± 1.08mV, n = 8; $EdCa_V\beta2$ $V_{a1/2}$ = -14.22 ± 1.46mV, n = 5; $CcCa_V\beta$ $V_{a1/2}$ = -18.47 ± 1.59mV, n = 6; $CxCa_V\beta$ $V_{a1/2}$ = -28.89 ± 1.54mV, n = 15; $PpCa_V\beta$ $V_{a1/2}$ = -15.29 ±

951 1.23mV, n = 10; $ChCa_V\beta$ $V_{a1/2}$ = -10.30 ± 1.04mV, n = 12. $rCa_V\beta2$ $V_{i1/2}$ = -2.98 ± 13.51mV, n = 12;
952 $NveCa_V\beta$ $V_{i1/2}$ = -68.93 ± 1.53mV, n = 5; $EdCa_V\beta1$ $V_{i1/2}$ = -56.76 ± 3.18mV, n = 8; $EdCa_V\beta2$ $V_{i1/2}$ =
953 -18.84 ± 8.00mV, n = 5; $CcCa_V\beta$ subunit $V_{i1/2}$ = -47.81 ± 5.57mV, n = 6; $CxCa_V\beta$ $V_{i1/2}$ = -87.75 ±
954 1.72mV, n = 15; $PpCa_V\beta$ $V_{i1/2}$ = -99.80 ± 0.92mV, n = 10; $ChCa_V\beta$ $V_{i1/2}$ = -70.25 ± 4.67mV, n = 12.
955 **C)** Diagram of Ca_V β subunit domain swaps and the length of the N-terminus swapped in amino
956 acids.
957 **D)** Cnidarian Ca_V β N-termini do not greatly affect voltage-dependent activation of Ca_V channels
958 containing $EdCa_V\beta2$. Voltage-dependent activation ($V_{a1/2}$) of heterologously-expressed Ca_Vs with
959 WT $EdCa_V\beta2$, β subunits from the indicated cnidarians, and chimeras with their N-termini on
960 $EdCa_V\beta2$, p = 0.5830 for average $V_{i1/2}$ values across mutant beta subunits, one-way ANOVA with
961 Bartlett's test and post-hoc Tukey test, n = 4-7 cells. Data represented as mean ± sem.

962 **Figure 5 Supplementary Table 1: Wild type and Chimeric $Ca_V\beta$ amino acid sequences.**